



Carbon dioxide–brine–rock interactions in a carbonate reservoir capped by shale: Experimental insights regarding the evolution of trace metals

Virginia Marcon ^{a,1}, John P. Kaszuba ^{a,b,*}

^a Department of Geology and Geophysics, 1000 E. University Avenue, University of Wyoming, Laramie, WY 82071, USA

^b School of Energy Resources, 1000 E. University Avenue, University of Wyoming, Laramie, WY 82071, USA

Received 24 April 2014; accepted in revised form 27 June 2015; available online 2 July 2015

Abstract

Trace metal behavior provides important information regarding fluid–rock interactions in CO₂-charged water–rock systems and constrains potential environmental impacts. Hydrothermal experiments evaluated mechanisms of release, evolution, and subsequent scavenging of trace metals at 160 °C and 25 MPa. Experiments were designed to simulate two theoretical locations within a CO₂-charged reservoir: (1) at the contact between a shale caprock and carbonate reservoir and (2) deeper within a carbonate reservoir, away from the shale.

CO₂ injection into brine (ionic strength = 3.3 mol/kg) decreased the pH by 1–2 units; concomitant mineral dissolution elevated Ba, Co, Cu, Pb, and V concentrations in the brine at both simulated locations within the reservoir. Additionally, Fe, Ni, and Zn concentrations increased in the mixed shale-carbonate experiment; Ba and Cd concentrations increased in the carbonate-only experiment. However, concentrations of Fe, Ba, Cr, and Pb in the mixed shale-carbonate experiment and Cr, Pb, V, and Zn within the carbonate-only experiment subsequently decreased as a result of precipitation of sulfides (Fe and Co sulfides), oxides, and clays. At the conclusion of the experiments, Fe, Pb, and Cr exceeded U.S. Environmental Protection Agency maximum contaminant limits in both experiments. In addition, zinc exceeded the limits at the simulated shale-carbonate contact and Ba, Cu, and Cd exceeded the limits in the simulated carbonate reservoir. Experimentally observed trends of decreasing Fe and Pb concentrations suggest these trace metals become less of an environmental concern as CO₂–water–rock reactions evolve with time.

The shale caprock plays an active role in trace metal evolution. The shale is a large source of metals, but also provides metal sinks such as primary clays, secondary smectites, and other silicates that are not found deeper within the carbonate reservoir, away from the shale. This potential mechanism of self-healing mitigates, but does not eliminate, the possible impact of trace metals in CO₂-charged systems such as carbon sequestration reservoirs.

© 2015 Elsevier Ltd. All rights reserved.

1. INTRODUCTION

Development of fossil fuels, emission of greenhouse gases, and changing climate have been at the forefront of geopolitical discussions in recent years. The challenge is to produce enough energy to maintain the current standard of living while simultaneously reducing greenhouse gas (GHG) emissions. As conventional oil and gas reservoirs

* Corresponding author at: Department of Geology and Geophysics, 1000 E. University Avenue, University of Wyoming, Laramie, WY 82071, USA. Tel.: +1 (307) 766 6065; fax: +1 (307) 766 6679.

E-mail addresses: vmarcon@incontroltech.com (V. Marcon), John.Kaszuba@uwyo.edu (J.P. Kaszuba).

¹ Present address: InControl Technologies, Inc., 3845 Cypress Creek Parkway Suite 195, Houston, TX 77068, USA.

are reaching the end of their life, society has turned to enhanced oil recovery and enhanced gas recovery (EOR and EGR, respectively) in order to retrieve oil that cannot be produced during the first stages of production. Multiple methods are used to enhance the recovery of oil and gas, including chemical flooding, thermal processes, and immiscible displacement by injection of CO₂ (i.e. CO₂ floods). Injection of CO₂ not only provides significant quantities of needed fossil fuels, but also may aid in mitigation of anthropogenic CO₂ by serving as a geologic carbon sequestration (GCS) strategy.

A significant amount of geochemical research has been conducted in recent years to understand CO₂–water–rock interactions in EOR, EGR, and especially GCS systems; much of this research has focused on changes in the composition of formation waters, mineral dissolution and precipitation, productivity of the reservoir, and modification of the porosity/permeability network (Kaszuba et al., 2005; Benson and Cole, 2008; Newell et al., 2008; Birkholzer and Zhou, 2009; Credoz et al., 2009; Kaszuba and Janecky, 2009; Kharaka et al., 2009; Lu et al., 2009, 2010a,b; Alemu et al., 2011; Liu et al., 2012; Qafoku et al., 2012; Schoonen et al., 2012; DePaolo et al., 2013 and references therein). However, CO₂–water–rock interactions are potentially important in a number of other anthropogenic and natural environments. For example, CO₂ is being evaluated as a working fluid in enhanced geothermal systems (EGS) (Pruess, 2006). Additionally, CO₂–water–rock interactions influence the geochemistry of natural CO₂ reservoirs, CO₂-bearing petroleum systems, and CO₂-charged thermal springs.

CO₂ can be contained in permeable formations and reservoirs that are capped by an impermeable or low permeability formation such as shale in natural CO₂ reservoirs (e.g. Allis et al., 2001), petroleum systems, and GCS reservoirs. Small discontinuities in the caprock along faults, fractures, and/or wells, as well as lateral heterogeneities, could allow CO₂-charged formation water containing metals and CO₂ to migrate into an overlying potable aquifer (IPCC, 2005; Humez et al., 2011, 2013; Keating et al., 2013c). The potential migration of CO₂ in a GCS scenario brought forth a wave of field, modeling, and experimental studies to investigate the conditions in which CO₂ migrates, and to evaluate potential impacts on potable waters overlying GCS reservoirs (Humez et al., 2011; Lions et al., 2014). Field studies of natural analogues provide an understanding of how systems have historically responded to the natural intrusion of CO₂ and/or CO₂-saturated brine (e.g. Keating et al., 2010, 2013a,c; Han et al., 2013). Additionally, field studies have been used to develop new monitoring techniques (measurement, verification, and accounting or MVA) for detecting leaks, simulate CO₂ leakage into a potable aquifer, and investigate how CO₂ would impact potable water sources (e.g. Smyth et al., 2009; Keating et al., 2010, 2013a; Kharaka et al., 2010; Trautz et al., 2013; Humez et al., 2014; Rillard et al., 2014). Modeling studies were developed to better understand the physicality, fluid dynamics, and risks associated with leaking brine and/or CO₂ into an overlying potable aquifer (e.g. Wang and Jaffe, 2004; Nicot and Duncan,

2008; Birkholzer and Zhou, 2009; Birkholzer et al., 2009; Zheng et al., 2009; Wilkin and Digiulio, 2010; Walter et al., 2012; Wunsch et al., 2013a; Keating et al., 2013c). Even though natural analogue and GCS modeling studies show that both CO₂ and CO₂-saturated brine can migrate from a reservoir into overlying water sources, experimental research has predominantly focused on the impact of CO₂ to potable aquifers (e.g. Smyth et al., 2009; Little and Jackson, 2010; Lu et al., 2010b; Rempel et al., 2011; Bearup et al., 2012; Karamalidis et al., 2013; Wunsch et al., 2013a,c,f; Kirsch et al., 2014).

The addition of CO₂ into a formation decreases pH by 1–2 units (Kaszuba et al., 2005; Little and Jackson, 2010), leading to changes in chemical reaction rates, dissolution of minerals (Bandstra and Brantley, 2008) and release of metals (e.g. Ba, Cd, Co, Cu, Fe, Pb, Ni, and V) (Liu et al., 2012; Wunsch et al., 2013c,f; Kirsch et al., 2014; Lions et al., 2014). Trace concentrations of many of these metals are associated with human health concerns. The United States Environmental Protection Agency (EPA) has set concentration limits, a maximum contaminant level (MCL), in groundwater for Sb, As, Ba, Be, Cd, Cr, Cu, F, Pb, Hg, NO₂, NO₃, Se, Tl, and U in order to mitigate potential human health impacts. In addition, the EPA has set secondary limits for Al, Cl, Fe, Mn, Ag, SO₄, and Zn, which are based on aesthetic qualities (Environmental Protection Agency, 2012). Nickel is not currently regulated by the EPA but is regulated by the European Union and World Health Organization (WHO) and is associated with adverse health implications (European Parliament and Council, 2000; World Health Organization, 2011; Lions et al., 2014). Nickel can be found at elevated levels in CO₂-water–rock systems such as oil field brines (Collins, 1975). Metals that exceed the EPA'S MCL and are not sequestered by secondary mineralization are considered a larger risk and more likely to be transported by CO₂-saturated brine to an overlying potable aquifer. Understanding the evolution of metals in CO₂-saturated brine within a reservoir is important because: (1) trace metals can be used as an indicator for geochemical processes that cannot be resolved by major element geochemistry, (2) trace metals from the reservoir provide a potential source of contamination to a potable aquifer, and (3) a basic knowledge of long-term CO₂–water–rock interactions is helpful when determining risk and overall evolution of a carbonate reservoir, particularly the response and recovery of a reservoir after CO₂ injection has ceased.

The purpose of this paper is to evaluate the evolution of trace metals in brine that becomes saturated with CO₂. For this study, geochemical experiments evaluated mechanisms of release, evolution, and subsequent scavenging of metals at in-situ conditions within a simulated, CO₂-charged carbonate formation and overlying shale (Fig. 1), a common geologic setting in sedimentary basins. Multi-component analyses on mineralogy and inorganic aqueous chemistry were completed to quantify and understand metal evolution.

In our experiments, metal concentrations (i.e. Cu, Pb, Fe, Zn, and Ni) initially increase in the brine as a result of injecting supercritical CO₂, which is consistent with

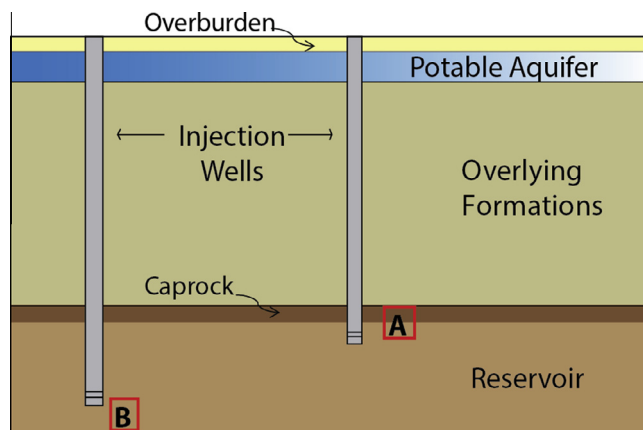


Fig. 1. This general cross-section is a conceptual model of a carbonate reservoir overlain by shale that the hydrothermal experiments simulate. The experiments investigate fluid–rock interactions at two locations: (A) at the shale–carbonate contact (ShaleBrine and ShaleCO₂), and (B) deeper within the carbonate reservoir, away from the shale caprock (CarbBrine and CarbCO₂). This cross-section is not drawn to scale.

experimental investigations of CO₂ leakage from GCS reservoirs into potable aquifers (i.e. Smyth et al., 2009; Little and Jackson, 2010; Lu et al., 2010b; Bearup et al., 2012; Karamalidis et al., 2013; Trautz et al., 2013,c,f; Kirsch et al., 2014). However, with some exceptions (most notably Ba, Cr, Pb, Fe in the carbonate–shale experiments and Cr, V, Zn, and Pb in the carbonate experiments), we observe a subsequent decline in the concentration of many of these trace metals that can be attributed to secondary mineral precipitation and/or sorption of metals onto mineral surfaces. These results are directly relevant to understanding CO₂–water–rock interactions and the mobility of trace metals in systems where CO₂ is prevalent (e.g. GCS, EOR/EGR, and EGS systems). These results also provide insight into fluid–rock interactions in a range of natural geologic systems including natural CO₂ reservoirs, CO₂-bearing petroleum systems, and CO₂-charged thermal springs. Additionally, the development of unconventional shale gas and oil through hydraulic fracturing targets many of the same formations associated with GCS and shares similar attributes and risks such as early acid-dominated reactions and potential risks to groundwater through similar leakage pathways (Nicot and Duncan, 2012). Therefore, our results also provide insight to the mobility of trace metals in this burgeoning method for hydrocarbon production.

2. EXPERIMENTS AND GEOCHEMICAL MODELS

2.1. Geologic setting

The suite of experiments is a proxy for a CO₂-charged carbonate formation overlain by shale. The experimental design encapsulates the essential features of a CO₂-charged carbonate–shale sequence in the Greater Aneth Field in the Paradox Basin, southeast Utah (Fig. 2A). We selected this geologic setting to guide our experiments because it is well characterized and is representative of carbonate–shale sequences common to sedimentary basins. In addition, elevated levels of salinity (145–17,300 mg/l – varying spatially) have been reported

for the overlying potable aquifer, which in some cases have been correlated with the start of oil and gas exploration in the region (Avery, 1986; Spangler et al., 1996). Therefore, our results are broadly applicable to other sedimentary basins where carbonate–shale sequences are overlain by a potable aquifer.

The Pennsylvanian Desert Creek Limestone, an evaporitic carbonate sequence, is the main hydrocarbon reservoir within the Greater Aneth Field (Sarg, 1999; McClure et al., 2003). Oil is being produced from this field by means of EOR using CO₂ injection. This field is also a sequestration pilot site for the Southwest Regional Partnership on Sequestration (New Mexico Tech, 2012b). The organic rich Gothic Shale and Chimney Rock Shale are the sealing units above the Desert Creek Limestone (Fig. 2B). A total of ~140,000 tons of CO₂ per year for a 2 year pilot test were injected into the Desert Creek Limestone (New Mexico Tech, 2012a) at depths of 1707–1768 meters (Griffith et al., 2011).

A distinctive feature of the Greater Aneth Field is that it is located in a region where groundwater is the predominant supply of potable water. The Navajo Sandstone is the overlying shallow aquifer (McClure et al., 2003; Rutledge, 2010) at a depth of approximately 560 meters near the Aneth Field (Goode, 1958). The history of elevated salinity in the Navajo Formation suggests that potable aquifers in the region may be susceptible to incursion from deep basin fluids, such as metal-laden CO₂-saturated brine.

2.2. Experimental design and materials

Hydrothermal experiments reacted brine, idealized limestone, shale, and supercritical CO₂ at 25 MPa and 160 °C using experimental techniques developed in previous studies (Seyfried et al., 1987; Kaszuba et al., 2003, 2005; Chopping and Kaszuba, 2012). Experiments were conducted using a rocking autoclave system (rocker bombs) and a flexible gold Dickson-type cell (Seyfried et al., 1987). The temperature of the experiments (160°C) is greater than temperatures naturally found in the Desert Creek Limestone (55–70 °C)

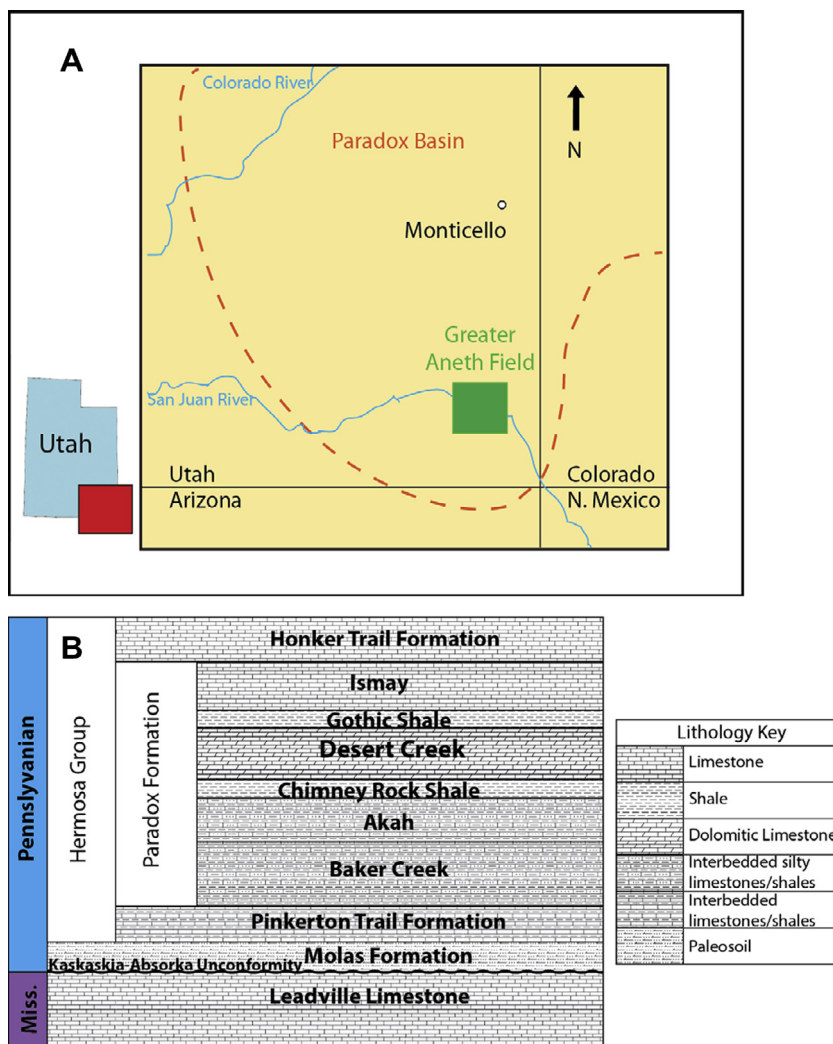


Fig. 2. The experimental design encapsulates the essential features of a CO_2 -charged carbonate-shale sequence in the Greater Aneth Field in the Paradox Basin, southeast Utah (image A); the Paradox Basin boundary is dashed. Image B shows a generalized stratigraphic column of the formations found within the Greater Aneth Field (modified from McClure et al., 2003). The geochemistry and mineralogy of the Desert Creek Limestone and the Gothic Shale guided the design of our experiments. The overlying potable aquifer in the region is the Navajo Sandstone (not shown).

(Manrique et al., 2004; Rutledge, 2010). The temperature of 160°C was chosen to accelerate kinetics; geochemical calculations suggest that the water–rock interactions are the same as those predicted at lower in-situ temperatures (EA Table 4). This approach is used in similar experimental studies (Gunter et al., 1997; Creodz et al., 2009; Alemu et al., 2011). Applying the general rule of thumb that every 10°C increase in temperature approximately doubles kinetic rates (Krauskopf and Bird, 1994), each experiment represents approximately 200 years of CO_2 -water–rock reaction at reservoir conditions.

Hydrothermal experiments focused on water–rock interactions at two theoretical locations within a carbonate reservoir: at a carbonate–shale interface (experiments designated as ShaleBrine and Shale CO_2) and within a carbonate reservoir away from a shale caprock (experiments designated as CarbBrine and Carb CO_2) (Fig. 1). ShaleBrine

and Shale CO_2 experiments contain 50% idealized limestone (1:1 calcite and dolomite with 1% pyrite) and 50% Gothic Shale mixed together (Table 1). CarbBrine and Carb CO_2 contain only idealized limestone (Table 1). The experiments replicated water–rock interactions before (ShaleBrine and CarbBrine, water–rock experiments) and after (Shale CO_2 and Carb CO_2 , water–rock- CO_2 experiments) CO_2 is introduced. These batch experiments are analogous to a location away from the source of CO_2 , along the fringe where CO_2 is displacing water and flow rates are negligible. Shale CO_2 and Carb CO_2 reacted for approximately 28 days to allow the brine to approach steady state with respect to the minerals (henceforth referred to as water–rock portion) before CO_2 was added. Supercritical CO_2 was then injected at a constant flow rate and the experiments subsequently reacted for approximately 48 days (henceforth referred to as water–rock- CO_2 portion). The mass of CO_2 needed to

Table 1
Experimental parameters and mineral compositions.

Experiment	ShaleBrine	ShaleCO ₂	CarbBrine	CarbCO ₂
Description	Shale–carbonate reservoir interface: water + Ls + Shale	Shale–carbonate reservoir interface: water + Ls + Shale + scCO ₂	Deep carbonate reservoir: water + Ls	Deep carbonate reservoir: water + Ls + scCO ₂
Initial pH	6.4 ± 0.1	6.6 ± 0.1	6.3 ± 0.1	6.7 ± 0.1
Temperature (°C)	160.3 ± 0.3	160.4 ± 0.8	160.3 ± 0.3	160.0 ± 0.4
Pressure (MPa), Pre-scCO ₂ injection	25.0 ± 3.5	24.6 ± 1.3	24.4 ± 2.6	25.4 ± 0.4
Pressure (MPa), Post-scCO ₂ injection	N/A	38.4 ± 5.4	N/A	37.8 ± 1.0
Initial water:rock ratio ^a	21:1	21.5:1	22:1	21.5:1
Rock mass ^b	11.50	11.03	10.83	10.88
Mineral proportions (Cc:Do:Py:Sh)	33:33:4:30	31:31:2:36	48:48:4:0	47:47:5:0
Water–rock reaction time (hours)	1028	673	745	676
Water–rock–scCO ₂ reaction time (hours)	N/A	1157	N/A	815
Total reaction time (hours)	1028	1830	745	1491
Surface area of unreacted powders (m ² /g)	3.2914 ± 0.1920	3.2914 ± 0.1910	0.5394 ± 0.0170	0.5394 ± 0.0180
Surface area of reacted powders (m ² /g)	2.3767 ± 0.0285	1.5442 ± 0.0203	0.2550 ± 0.0110	0.2106 ± 0.0116

scCO₂ = supercritical CO₂; N/A = not applicable; Ls = limestone; Cc = calcite; Do = dolomite; Py = pyrite; Sh = shale.

^a Ratio decreases by approximately 1.4 by termination.

^b Rock mass input into reaction cell.

ensure that two immiscible fluid phases exist throughout the duration of the experiment was calculated using an equation of state (Duan et al., 2006). In order to replicate the pressure increase seen in the field (Birkholzer and Zhou, 2009; Birkholzer et al., 2009; Schaefer et al., 2012), experimental pressure was allowed to increase in response to CO₂ injection. As CO₂ slowly dissolved into the brine, pressure decreased and stabilized approximately 24 h after injection. Table 1 summarizes experimental parameters for this study.

The starting brine was based on natural conditions found within the Desert Creek Limestone; the ionic strength was 3.3 molal and the pH was 6.5. To synthesize the brine, research-grade salts and standards were mixed with deionized water and sparged of dissolved oxygen and carbon dioxide to control redox state. The initial brine composition was calculated to be in equilibrium, or as close as possible, with the minerals used in the experiments in order to minimize reaction between the minerals and brine prior to injection of CO₂. All four experiments used the same initial brine composition. A fifth experiment reacted 3 molal NaCl brine without rock at 25 MPa and 160 °C for approximately 250 h. This “blank” experiment evaluated whether the experimental apparatus contributed metals to the experiments; all metal concentrations were considered negligible compared to values measured in the experiments.

Aqueous samples were collected to evaluate changes in major and trace element water chemistry, dissolved total inorganic carbon (ΣCO₂), and pH. Samples were collected frequently early in the experiment and after introduction of CO₂ to capture rapid geochemical changes; subsequent sampling was less frequent to monitor later geochemical changes. U.S. EPA MCLs and secondary drinking water regulations were used as a metric to evaluate these aqueous data. Here we make a conservative assumption that metals exceeding the regulatory limit at the source (i.e. within the simulated carbonate reservoir) have the greatest likelihood to exceed regulatory limits in a potable aquifer due to

migration of metal-bearing brine. This assumption does not consider advective, reactive, or biogeochemical processes that may reduce the concentrations along a migration pathway (Lions et al., 2014).

Gothic Shale core sample (GS 5391) was used in the experiments to provide a realistic caprock. The Gothic Shale is a sapropelic (organic rich) dolomite and dolomitic shale to silty carbonate mudstone (Goldhammer et al., 1994) consisting of minor quartz, calcite, dolomite, and mica in a predominantly clay matrix with authigenic pyrite (Heath et al., 2011) (Table 2). An idealized Desert Creek Limestone consisting of 48 wt% calcite, 48 wt% dolomite, and 4 wt% pyrite (Table 2) was used as the reservoir to reduce complexities that are found in a natural limestone, such as preexisting alteration minerals, complex biogenic materials, and heterogeneous composition. The rocks and minerals used in the experiments consisted of 75 weight percent powder (<45 microns) to enhance reaction kinetics, and 25 weight percent fragments (~20–30 mm) for textural analysis.

2.3. Analytical methods

Major cation, anion, and trace constituent concentrations in the aqueous samples were determined by inductively-coupled plasma optical emission spectroscopy (ICP-OES), ion chromatography (IC) and inductively-coupled plasma mass spectrometry (ICP-MS), respectively. Additionally, pH and total inorganic carbon were analyzed using the methods of Chopping and Kaszuba (2012) as described in detail in Marcon (2013). Total dissolved inorganic carbon was measured for both “bench” (degassed samples at 25 °C and 0.1 MPa) and in-situ conditions; this data was used to calculate in-situ pH as described by Newell et al. (2008) and Chopping and Kaszuba (2012). Unreacted and reacted minerals and rocks were analyzed using X-ray diffraction (XRD), optical microscopy, field emission scanning electron microscopy (FESEM), energy

Table 2
Mineralogy of the Gothic Shale, Desert Creek Limestone, and idealized limestone used in the experiments.

	Gothic (5391) ^a	Desert Creek Limestone	Idealized limestone
Illite	X	O	
Smectite	X	O	
Quartz	O	X	
Calcite	O	X	X
Dolomite	O	X	X
Pyrite	O	O	O
Mica	O		
Kaolinite		O	

O = minor component; X = major component.

^a Heath et al. (2011) and XRD performed for this study.

dispersive analysis system (EDS) and ICP-OES following acid digestion. The methods are described in detail in Marcon (2013).

Upon termination, or “quench”, experiments were cooled as quickly as possible to minimize retrograde reactions of the fluids and rocks. The starting brine and recovered, reacted brine were filtered using a Millipore 0.45 µm filter and analyzed according to the same protocols as the other samples. The compositions of unreacted and reacted minerals were analyzed and compared to determine mineral reactions and metal mobility as a result of water–rock–CO₂ interactions. The geochemistry of the quench sample and the aqueous sample collected immediately prior to the quench was compared to determine retrograde reactions that occurred while cooling and degassing the experiments.

2.4. Statistical analysis

A statistical analysis of the aqueous chemistry was performed using QualStat 6.0 (Callahan and Marcon, 2013) to determine correlations between various analytes and develop regression equations and trend analyses for the experimental results. Correlation of each constituent was reviewed versus time before, after, and through addition of CO₂. A correlation coefficient greater than 0.7 ($p < 0.05$) was considered a strong correlation and suggested a temporal relationship within the system.

Because of the nature of the experimental design, the study has a limited number of observations. The capability to detect a statistical difference is based on the number of observations within each experiment ($n \geq 8$); the more samples included, the greater the ability to detect a statistical difference. The power of the statistical test was improved by including duplicate samples (i.e. sample 5 in ShaleCO₂ and CarbCO₂) as well as duplicate analyses in the various sample groups; the use of duplicates provides a higher degree of confidence in the experimental outcomes. Due to the limited number of observations within each sample group, only the constituents that exhibited a strong correlation could be identified as different from the background. Supplementary trends were estimated visually using aqueous chemistry plots (Figs. 3 and 4). Individual analytes were also correlated to each other to help differentiate the source of metal release between the caprock and storage reservoir.

Student *t*-test was used to compare concentrations of each constituent before (samples 3, 4, and 5 of each experiment) and after (samples 6, 7, and 8 of each experiment) CO₂ is added (EA Table 3). Comparing interval groups before and after injection provided a way to determine the greatest impact made by injecting CO₂. The experiments approached a steady state condition around 115 h (sample 3); (Figs. 3 and 4) therefore, samples 3 through 5 were selected to represent pre-injection aqueous fluid compositions. Again, duplicate aqueous samples for individual water samples were considered within these analyses to increase the power of the statistical test. The same approach was used for post-injection samples. The major proportion of reaction progress and metal release occurred within 120 h after injection of CO₂; changes in chemistry diminished around 800 h (after sample 8). If a statistical difference was observed ($p < 0.05$), then a statistically significant change in concentration between the pre- and post-injection sample groups exists. The mean difference present in each sample group is greater than the overall analytical error for each individual sample and therefore a statistical difference can be observed.

2.5. Geochemical models

Geochemical models were developed to calculate initial brine compositions, determine equilibrium state of the system, calculate pH at experimental conditions (in-situ pH), calculate redox state, and interpret experimental results. Models were developed using Geochemist Workbench 9.0 (GWB), the b-dot ion association model, and the resident thermo.dat database (Bethke and Yeakel, 2012) according to methods described in Chopping and Kaszuba (2012) and Marcon (2013). We use thermo.dat because it is internally consistent and handles aluminum speciation more adeptly than other available databases (Kaszuba et al., 2011b). A nonstoichiometric, iron-bearing dolomite was added to the database to represent the dolomite used in the experiments (Table 3). Equilibrium constants for this dolomite were calculated using an ideal solution model between dolomite and ankerite (EA Table 1) (Anderson and Crerar, 1993). This approach has been used in other studies to account for iron in dolomite (Xu et al., 2004, 2005, 2007). Initial oxygen values were assumed to be negligible due to sparging of the brine.

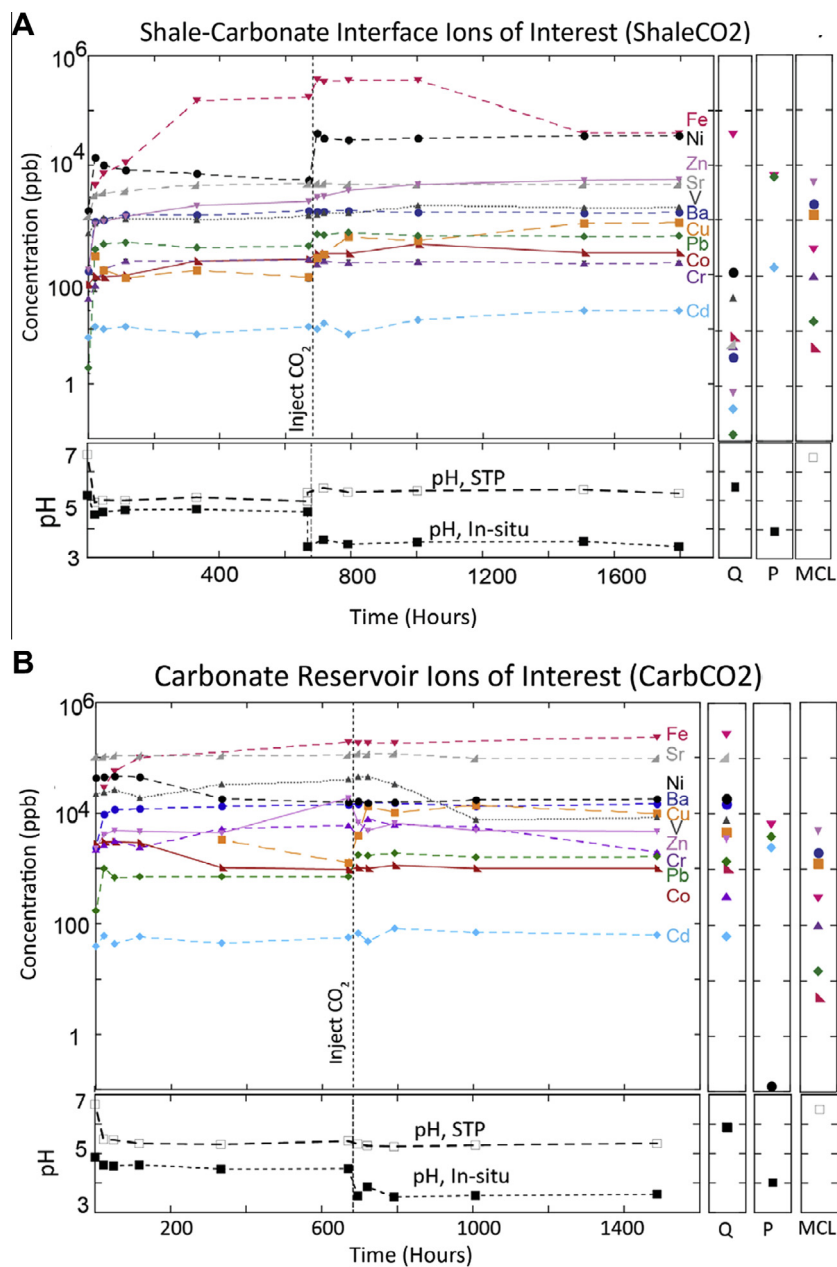


Fig. 3. Aqueous geochemistry versus time for select metals in ShaleCO₂ (A) and CarbCO₂ (B). The brine and rocks are allowed to approach steady state at 160 °C and 25 MPa for approximately 28 days before CO₂ is injected (represented by the vertical dashed line). After CO₂ is injected (to the right of the dashed line), the experiments are allowed to react for approximately 45 days to monitor chemical changes as a result of CO₂–water–rock interactions. Notice an increase in concentration for Ba, Fe, Ni, and Pb in ShaleCO₂ and Cu, Fe, Pb, and V in CarbCO₂ immediately after injection. This increase is followed by a subsequent decline in concentration with time. In the box next to each aqueous plot, the sample collected after the experiment is terminated, or “quenched” (25 °C and 0.1 MPa, denoted by ‘Q’), and predicted concentrations (P) are reported. For a comparison, the EPA MCLs for primary and secondary elements are in the box to the far right. In-situ (solid squares) and bench (open squares) pH are plotted below the aqueous trends capturing an initial decrease in pH after injection. Again, quench (Q) and predicted (P) values are plotted to the right; the MCL is for surface waters and not applicable for deep formations. The mean standard error is plotted for each sample (in most cases the error bars are the size of the symbols and therefore, cannot be seen). EA Fig. 1 depicts the sample collected immediately before CO₂ injection and the three samples collected immediately after injection to illustrate the visual change. “pH, STP” denotes pH measured at the bench (25 °C and 0.1 MPa).

Predictive models calculate the thermodynamic end state to which the experimental system will ultimately evolve. These calculations identify secondary minerals that are thermodynamically favored to precipitate as well as

aqueous species concentrations. In the predictive model, Gothic Shale was represented as 25% illite, 25% smectite, and 10% each calcite, dolomite, pyrite, quartz, and mica (Table 2). Predicted equilibrium concentrations and the

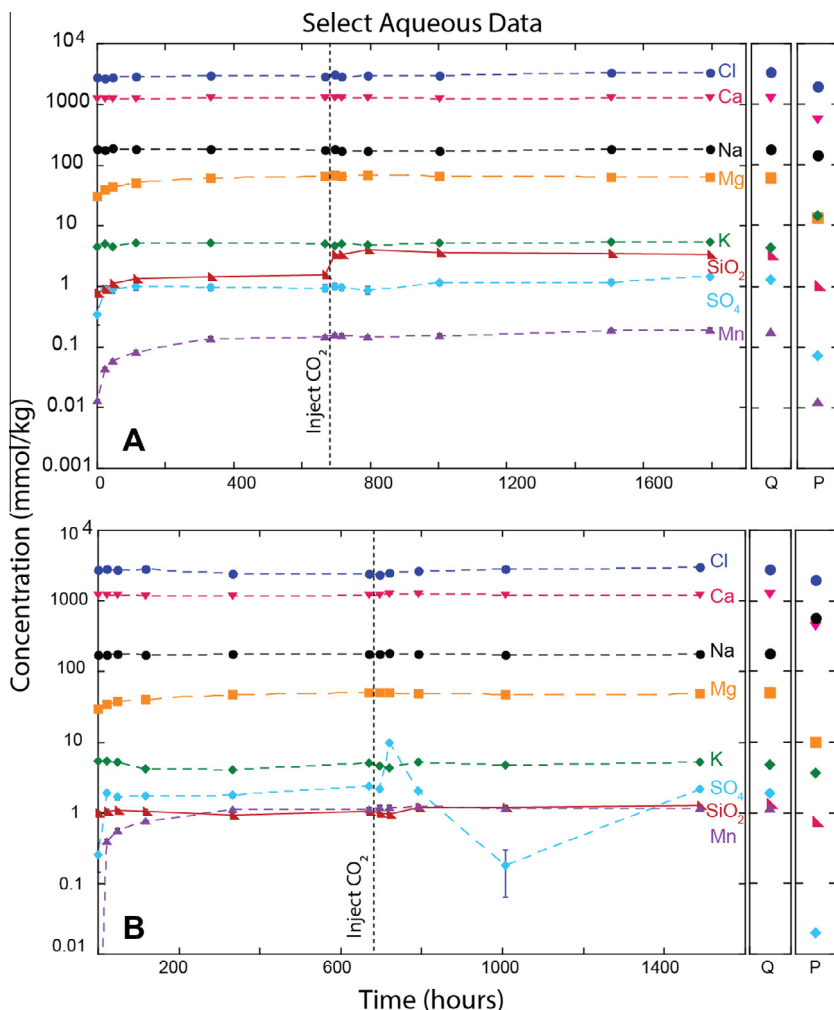


Fig. 4. Aqueous geochemistry versus time for select analytes in ShaleCO₂ (A) and CarbCO₂ (B). Prior to CO₂ injection (represented by the dashed line), brine and rocks react and approach a steady state at 160 °C and 25 MPa. The water is monitored over time, up to 45 days, for change in chemistry indicative of water–rock–CO₂ reactions. The mean standard error is plotted for each sample. In most cases the error bars are the size of the symbols and therefore, cannot be seen.

composition of the final sample collected before terminating the experiment were compared to evaluate reaction progress within each experiment. Finally, in-situ pH, saturation indices (SI), and activities of aqueous species were calculated for each sample in all four experiments.

3. RESULTS AND DISCUSSION

3.1. Geochemical data

Chemical compositions of minerals and rocks used in the experiments, including major, minor, and trace metal contents, are tabulated in Table 3. Total values for the shale are low because CO₂ and organic carbon content were not measured. Aqueous geochemical data for all four fluid–rock experiments are tabulated in EA Table 2. Figs. 3 and 4 show the evolution of select analytes as a function of time for ShaleCO₂ (mixed shale–carbonate water–rock–CO₂ experiment) and CarbCO₂ (carbonate water–rock–CO₂ experiment). Data from ShaleBrine and CarbBrine are

not plotted because results are statistically similar to the water–rock portion of ShaleCO₂ and CarbCO₂ ($p > 0.05$). Also plotted are the predicted aqueous concentrations, measured pH, and calculated in-situ pH values. EPA MCLs are plotted as a comparison.

3.2. Simulated Shale–carbonate reservoir interface (ShaleBrine and ShaleCO₂)

The experiments simulating the shale–carbonate reservoir contact (ShaleBrine and ShaleCO₂) exhibit an increase in SiO₂(aq), Fe, Mg, Ca, Al, Mn, Co, Sr, and Zn concentrations when the experiments first began (Figs. 3 and 4, EA Table 2), indicating that the brine and rock were not in equilibrium at the start of the experiment. However, concentrations approached steady state before CO₂ was injected. The experiment simulating injection near the shale–carbonate reservoir contact (ShaleCO₂) generated a statistically positive mean difference ($p < 0.05$) in SiO₂(aq), Fe, Na, and K concentrations as a result of injection. The main source of

Table 3
Chemical composition (Weight Percent Oxides) of minerals and rocks used in experiments.

Oxide ^a	Calcite (Cc)	Dolomite (Do)	Pyrite (Py)	Gothic Shale (Sh)
SiO ₂	–	–	–	43.16
TiO ₂	–	–	0.05	0.47
Al ₂ O ₃	–	–	0.05	11.02
Fe ₂ O ₃	–	–	–	4.02
FeO	–	6.82	60.00	–
MnO	0.02	0.18	–	0.02
MgO	0.02	19.24	0.05	4.10
CaO	57.94	28.58	0.57	15.88
Na ₂ O	–	–	–	0.55
K ₂ O	–	–	–	2.50
P ₂ O ₅	–	–	–	0.52
CO ₂	41.99	45.11	–	–
Total	99.97	99.93	–	82.25
Chemical formula	CaCO ₃	Ca _{0.49} Mg _{0.46} Fe _{0.091} CO ₃	FeS ₂	–
Source	Chihuahua, Mexico	Selasrann, Norway	Zacatecas, Mexico	Paradox Basin, Utah
<i>Trace metals (ppb)</i>				
As	158.80	136.43	240.45	15398.23
Ba	1412.60	172.02	3.15	126534.88
Cd	DL	DL	0.75	540.12
Co	2.20	48.97	648.44	16710.76
Cr	19.50	48.23	5.26	251046.92
Cu	127.70	406.75	131.69	27640.78
Ni	38.90	108.83	30.31	97676.99
Pb	9.30	8.89	166.07	7150.68
Sr	230.80	473.79	15.60	344874.80
V	305.20	310.02	61.60	99848.29
Zn	7.30	59.40	69.24	242516.23

DL = below detection limit.

^a Analysis by ICP-OES after acid digestion of mineral.

silica is from reaction of acidified, carbonated brine with the shale caprock. Additionally, silica impurities in the dolomite (up to 1% weight percent silica) may have contributed to the total silica concentration. As acidified, carbonated brine dissolved carbonate and silicate minerals, as well as organic material, the size of pores in the shale appeared to increase (Fig. 5). Approximately 300 h after injection, silica and iron concentrations begin to decrease and level off before termination of the experiment. Formation of secondary smectites and kaolinite, identified by FESEM (Fig. 6), XRD, and saturation index calculations, are attributed to decreasing concentrations of iron and silica. The formation of swelling clays is important to the overall permeability of the caprock. Concentrations of SO₄, K, and Mn show a statistically significant increase ($p < 0.05$) during the water–rock–CO₂ portion of the experiment (EA Table 3, Fig. 4) attributed to the dissolution of the shale caprock and carbonates. The predicted major ion concentrations, with the exception of potassium, are lower than the measured major ion concentrations in final sample at experimental conditions. The predicted difference suggests that the fluids and rocks had not fully equilibrated before termination of the experiment.

The metals Co, Cu, Ni, Pb, V, and Zn statistically increased (positive mean difference of $p < 0.05$) in concentration as a result of injecting CO₂ (EA Table 3, Fig. 3). Before CO₂ was added, the concentration of lead increased

from 3 to ~300 ppb, a value above the EPA MCL. The increase in lead was a result of disequilibrium between the water and rock in a laboratory environment. The concentration of lead approximately doubled (from ~300 to 600 ppb) as a consequence of injecting CO₂. This increase in lead concentration was followed by a subsequent decrease ~500 h after injection. Lead concentrations continued to decline through the termination of the experiment. Despite this decline, lead concentration remained above the EPA MCL at termination of the experiment. The concentration of barium was still increasing during the water–rock portion of ShaleCO₂ at the time CO₂ was injected (at ~670 h). This increasing trend is the same behavior observed in the parallel water–rock experiment (ShaleBrine, EA Table 2B). Barium concentrations in ShaleBrine continued to increase through the termination of the experiment at ~1000 h. The continual increase in concentration indicates that the experiments had not yet reached steady state with respect to barium before CO₂ was added. However, after the addition of CO₂, barium concentration decreased. The decreasing trend suggests that secondary precipitation and/or sorption removed barium from solution at the simulated shale-carbonate reservoir contact (ShaleCO₂) after CO₂ was added. Cadmium, Cu, and Zn concentrations (20.6, 785, and 5220 ppb, respectively) continued to increase during the water–rock–CO₂

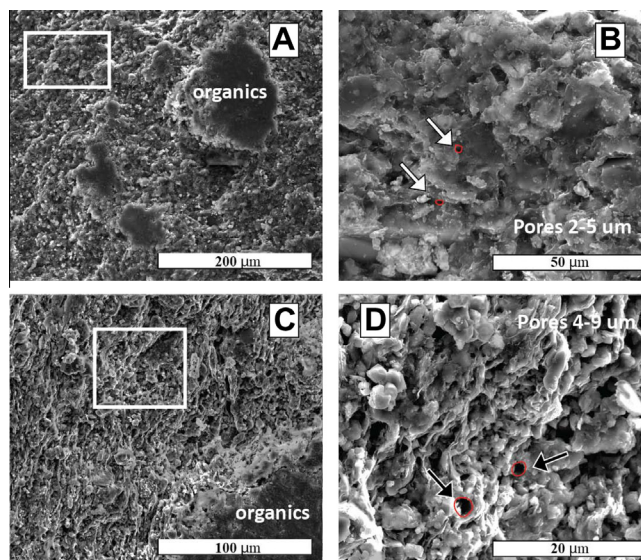


Fig. 5. FESEM images of Gothic Shale reacted with brine (Images A and B, ShaleBrine) and brine and CO₂ (Images C and D, ShaleCO₂). Image B shows an enlarged image of the box in image A, and image D is enlarged from the box in image C. Reaction with CO₂-saturated water suggests an approximate doubling of pore size (outlined in red) in the shale as result of silicate, carbonate, and organic matter dissolution. (For interpretation of the references to color in this figure legend, the reader is referred to the web version of this article.)

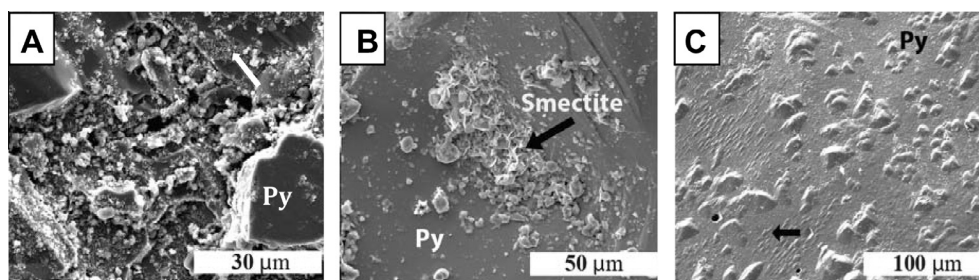


Fig. 6. FESEM micrographs of secondary minerals and dissolution textures on reacted pyrite (Py). Image A shows secondary Fe-metal-oxides (pointed out by the arrow) that precipitated in ShaleBrine (water–rock experiment emulating a shale–carbonate reservoir interface); these oxides contain V, Ni, and Co. After CO₂ is injected, Fe-oxides are no longer stable and release trace metals into solution. Image B shows secondary clay that precipitated during ShaleCO₂ and is interpreted to be smectite (based on XRD and EDS analyses). Image C captures the extensive dissolution (black arrow) observed for minerals in CarbCO₂, which represented deeper levels in the reservoir away from the caprock.

portion of the experiment (statistically significant increase at $p > 0.05$), but remained below EPA limits. After an initial increase, Co, Cr, and Pb concentrations all decreased in a similar pattern at ~500 h after injection. This trend suggests a similar process was controlling metal evolution for Co, Cr, and Pb, such as secondary precipitation and/or stoichiometrically equivalent sorption.

Predicted and measured trace metal concentrations do not agree as well as the predicted and measured major ion concentrations. Databases used in geochemical models, GWB included, do not accurately predict processes involving trace metals such as adsorption, ion exchange, and solid solution in minerals. Predicted concentrations represent thermodynamically favored endpoints, whereas these experiments are much more complex due to imperfect mineral structures and metal impurities. Because of these inconsistencies, the geochemical models are not perfectly representative of the steady state achieved by trace metals in the experiments.

3.3. Simulated carbonate reservoir (CarbBrine and CarbCO₂)

In the simulated carbonate reservoir, not in contact with a shale caprock (CarbCO₂), Ba, Fe, Mg, Mn, SO₄, and V concentrations increase during the water–rock portion of the experiment, whereas Ni, Cu, and Co concentrations decrease after an initial increase. After injection, none of the analytes indicate a statistically significant mean difference ($p > 0.05$) as a result of injecting CO₂. However, Cu, Pb, SO₄, and V visual trends (Figs. 3 and 4, EA Table 2) suggest an increase in concentration immediately after injection of CO₂. Approximately 120 h after injection, sulfate and vanadium concentrations subsequently decreased and SiO₂(aq) concentrations slightly increase. Iron concentrations gradually increased throughout the water–rock–CO₂ portion of the experiment to a concentration higher than pre-injection values. Again, predicted major

ion concentrations, with the exception of sodium, are generally lower than what was observed at the end of the experiment suggesting that the waters had not achieved equilibrium.

A significant mean difference ($p < 0.05$) was observed in Ba, Cu, Pb, and Sr, before and after the injection of CO₂, indicating a statistical change in metal mobilization as a result of injection (EA Table 3 and Fig. 3). After CO₂ was added, nickel concentrations increased ($r = 0.88$), and strontium ($r = -0.85$) and vanadium ($r = -0.86$) concentrations decreased. Lead concentrations remained below the EPA MCL during the water–rock portion, but increased above the EPA MCL after injection of CO₂ (from 70 to ~200 ppb). Forty-eight hours after injection, the concentration of lead slowly declined, but remained above the EPA MCL at the termination of the experiment; this trend is similar to ShaleCO₂. Barium concentrations in CarbBrine and CarbCO₂ exhibited similar behavior to the water–rock portion of shale-carbonate reservoir experiments. Conversely, barium concentrations continued to increase after the addition of CO₂ in CarbCO₂. The differing behavior of barium between the two experiments suggests that the presence of a clay caprock helps remove barium from the CO₂-charged brine.

3.4. Geochemical behavior at a Shale – carbonate reservoir contact versus a deep carbonate reservoir

Cadmium, Cu, Zn, and Pb exhibit similar geochemical trends within CarbCO₂. Similar trends in Zn, Cd, Cr, and Pb can be attributed to similar characteristics among these elements; they are all divalent cations, form complexes with organic matter, and are readily adsorbed to iron and manganese oxides (Drever, 1997). However, in ShaleCO₂, Cd and Zn show a different trend compared to Cr and Pb.

Lu et al. (2010b) performed similar experiments and reported the same declining trend as observed in our experiments. Lu et al. (2010b) also attributed the decrease in metal concentrations to re-adsorption of metals as pH recovers and stabilizes after the injection of CO₂; Humez et al. (2013) reported similar results. In addition to the role of adsorption/desorption associated with pH, we can also

attribute part of the declining concentrations to metals co-precipitating with sulfides and oxides (i.e. Fig. 7B Cu and Ni bearing pyrite).

Mineral dissolution textures, aqueous data, and secondary mineralization suggest that the dolomite and pyrite in CarbCO₂ (carbonate reservoir) reacted more extensively than in ShaleCO₂ (shale-carbonate reservoir contact) (Figs. 3, 4, 6 and 7). The reaction of additional silicate and carbonate minerals within the shale of ShaleCO₂ reduce the extent of dissolution of the limestone. Iron and barium concentrations both decline in ShaleCO₂ suggesting these elements are reincorporated within the rock. In contrast, CarbCO₂ iron (after an initial decrease) and barium concentrations continue to increase during the CO₂ portion of the experiment. Additionally, Cr, Cu, and Sr concentrations are elevated in CarbCO₂ compared to ShaleCO₂ even though additional metals are available within the shale. Although the shale provides an entirely new source of metals, it also provides additional sinks for metals to be removed from solution.

Formation of secondary minerals and adsorption help recapture metals that were mobilized by injection of CO₂. Carbonates, sulfates, and sulfides in the experiments, especially secondary metal-sulfides containing As, Ba, Co, Fe, and Ni, are possible sinks for these metals. Saturation state calculations (EA Table 4) demonstrate that the brine is saturated with respect to nickel-sulfides in ShaleCO₂ and CarbCO₂ after CO₂ was injected, as well as in the water–rock portion of ShaleCO₂. Arsenic and cobalt-sulfides precipitated in both CO₂ experiments after injection (Fig. 7B). The initial increase in iron in both ShaleCO₂ (right after injection) and CarbCO₂ (during the CO₂-water–rock portion of the experiment) can be attributed to dissolution of pyrite, iron-rich dolomite, and iron-rich clays (e.g. nontronite in ShaleCO₂) (Figs. 5–7). The subsequent decrease in iron concentration in ShaleCO₂ is attributed to precipitation of secondary clay (e.g. formation of smectites and vermiculite, ShaleCO₂ EDS and XRD data; Fig. 6B) as well as secondary pyrite (ShaleCO₂; Fig. 6) and siderite/ankerite (CarbCO₂). The composition of secondary minerals formed in ShaleBrine and ShaleCO₂, the two experiments that represent a carbonate-shale contact, are similar to carbonates

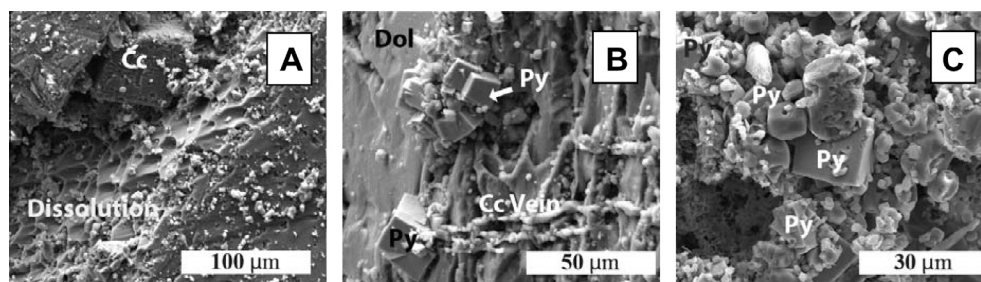


Fig. 7. FESEM micrographs of reacted mineral fragments. Image A illustrates dissolution textures on a calcite fragment in ShaleCO₂ (location A in Fig. 1, a shale-carbonate contact) as a result of CO₂-water–rock interactions; similar carbonate dissolution is also observed in CarbCO₂ (location B in Fig. 1, deeper within the carbonate reservoir). Images B and C show secondary cubic pyrite (Py), calcite (Cc), and a clay that precipitated on reacted dolomite (Dol) fragments in CarbCO₂. Whereas unreacted pyrite consisted of angular fragments, the pyrite shown in images B and C is cubic and thus is interpreted to have formed within the experiment. Ni and Cu co-precipitate with the secondary pyrite, which is consistent with the observed increase/decrease of aqueous trends before/after CO₂ is injected (Fig. 5).

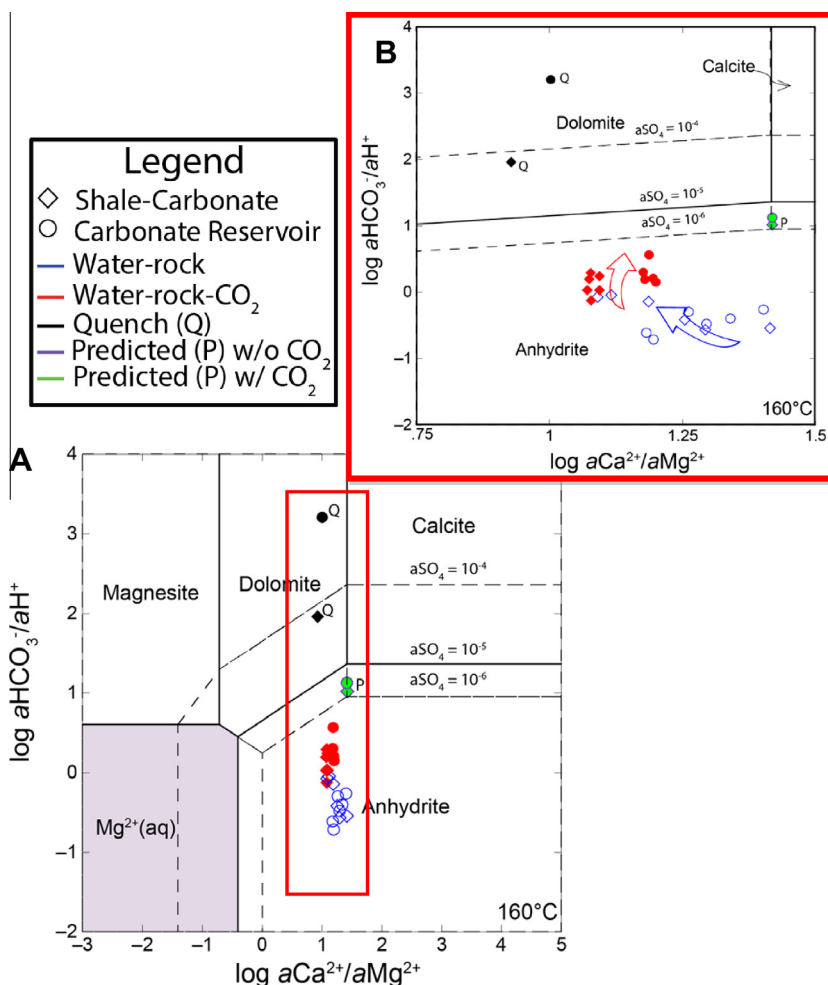


Fig. 8. Mineral stability relationship for the system CaO–MgO–CO₂ containing a range of SO₄ activity ($a_{\text{SO}_4} = 10^{-4}$, 10^{-5} , and 10^{-6}) at 160 °C and 25 MPa. Activities of aqueous species within individual samples, predicted equilibrium states (P), and quench samples (Q) are plotted on the diagram; the water–rock portion of the experiments are denoted by blue symbols and water–rock–CO₂ portion in red symbols. Arrows represent the general reaction paths. Image B is enlarged from the box in A. Carbonates are not stable and dissolve at experimental conditions (Fig. 4A), but precipitate during the cooling and degassing of the experiments (the quench) (Fig. 4B). The predictive calculations suggest that carbonates will stabilize when water and rocks approach equilibrium (blue circles at the junction of the calcite–dolomite–anhydrite stability fields). (For interpretation of the references to color in this figure legend, the reader is referred to the web version of this article.)

and sulfides observed in faults and fractures in the Desert Creek Limestone near its contact with the Gothic Shale (Tuttle et al., 1996). These similarities provide confidence that our experiments are a reasonable proxy for a carbonate–shale sequence.

After the experiments were terminated, the cooled, degassed waters were saturated with respect to barite, strontianite, copper–sulfides, and oxides containing Cu, Fe, and Zn. The cooling and degassing process in the laboratory is analogous to a scenario in which water migrates to the surface, reacting with the rocks and cooling and degassing along the flow path. The experiments suggest that these minerals may precipitate in such a scenario and provide a sink for sulfate and metals such as Ba, Cu, Cr, Zn, and Fe. Minerals enriched in these metals are commonly found in ore deposits such as Mississippi Valley Type (MVT), sedimentary exhalative (SEDEX), and red-bed coppers, all of which are proposed to have formed from movement of

basinal brines (Hitzman et al., 2005; Leach et al., 2005). These deposits are possible indicators of how migrating brine enriched in CO₂ may evolve. Additionally, our experiments can be used to shed light on these types of deposits and provide a basis for metal–brine relationships.

3.4.1. Dissolution of carbonate reservoir and mobilization of trace metals

CO₂ injection into deep saline formations acidifies the water through dissolution of CO₂ and formation of carbonic acid. Increased acidity drives the system away from equilibrium, and results in partial dissolution of rocks and minerals (Figs. 5, 6C, and 7A). In all of the experiments, carbonates dissolved during both the water–rock and water–rock–CO₂ portions of the experiments. However, more extensive calcite dissolution occurred in the experiments containing supercritical CO₂ (Fig. 7A). An activity diagram was constructed to investigate

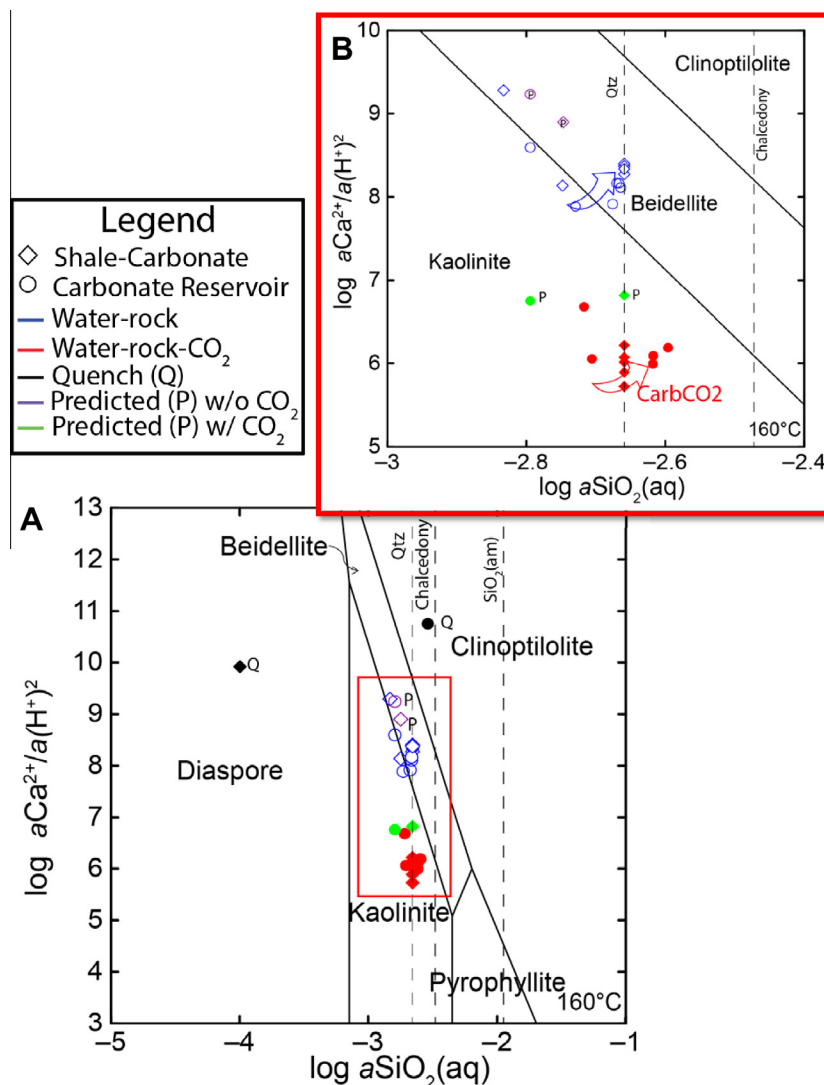


Fig. 9. Mineral stability relationships for the system $\text{Ca}_2\text{O}-\text{Al}_2\text{O}_3-\text{SiO}_2-\text{H}_2\text{O}$ at 160 °C at 25 MPa. Activities of aqueous species within individual samples, predicted equilibrium states (P), and quench samples (Q) are plotted on the diagram; the water–rock portion is denoted by blue symbols and water–rock- CO_2 portion in red symbols. The dashed vertical lines represent saturation with respect to: quartz (Qtz), chalcedony, and amorphous silica ($\text{SiO}_2(\text{am})$). The box in Figure A is enlarged in B; the arrows denote the general reaction paths. Silica activity near the shale-carbonate reservoir contact is controlled by the precipitation of quartz whereas deeper in the carbonate reservoir, away from the shale, the silica activity is only supplied from dissolution of inclusions within the dolomite. No secondary silicates precipitate deeper within the carbonate reservoir thus removing a potential metal sink. (For interpretation of the references to color in this figure legend, the reader is referred to the web version of this article.)

CO_2 –water–rock interactions and carbonate disequilibrium (Fig. 8). Throughout the duration of the experiments, the waters are saturated or supersaturated with respect to anhydrite. However, during the quenching process, the fluid becomes undersaturated with respect to anhydrite; no anhydrite was observed. In both of the experiments injected with supercritical CO_2 , the fluids are saturated with respect to carbonates only after the quenching process (Fig. 7B and 8, quench samples plot within the dolomite field). Calcite is a known sink for metals such as Ba, Cd, Co, Ni, Pb, and Sr through ion substitution, adsorption, lattice defects, solid or liquid inclusions, and/or

interstitially along crystal boundaries (Tucker and Wright, 1990). Formation of secondary carbonates during the termination process (Fig. 7) suggests that secondary carbonates may also precipitate during depressurization and degassing of migrating brine in a natural system; formation of secondary carbonates can help remove metals such as iron and lead from the solution. Finally, the predicted equilibrium values from experiments with and without supercritical CO_2 plot in the same location on the activity diagram (Fig. 8). The identical predicted values can be attributed to the congruent nature of carbonate dissolution; this will be discussed further in Section 3.4.3.

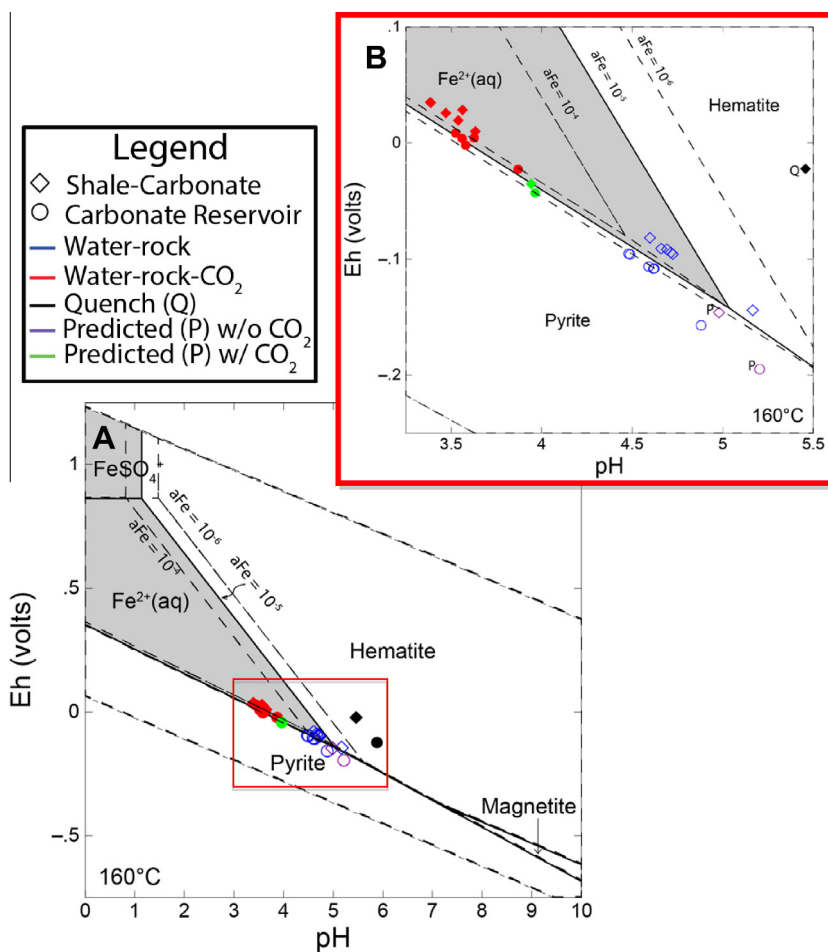


Fig. 10. Eh/pH stability diagram for Fe-SO₄-H₂O in the presence of CO₂(aq) (activity = 10⁻⁴) at a range of iron activities (10⁻⁶, 10⁻⁵, and 10⁻⁴). Activities of aqueous species within individual samples, predicted equilibrium states (P), and quench samples (Q) are plotted on the diagram; the water-rock portion is denoted by blue symbols and water-rock-CO₂ portion in red symbols. Figure B is enlarged from the box in A. After injection of CO₂, Fe-oxides destabilize and pyrite becomes stable (Fig. 5A). A siderite stability field does not appear until CO₂ activity exceeds 10⁻².

3.4.2. Recapturing mobilized metals

An additional activity diagram was developed to investigate CO₂-water-rock interactions with respect to calcium-aluminum silicates (Fig. 9). The water-rock portions of the two experiments follow similar reaction paths to the quartz saturation boundary within the beidellite (Na, Ca dioctahedral smectite) field. After the addition of CO₂, the reaction path transitions from within the smectite stability field to the kaolinite stability field. The reaction path at a simulated shale-carbonate reservoir contact (ShaleCO₂) transitions along the quartz stability boundary into the kaolinite field; this path is consistent with dissolution of primary smectites after CO₂ injection. Saturation index calculations (EA Table 4) suggest that the waters are saturated with respect to smectite prior to the injection of CO₂ at the simulated reservoir-caprock contact; however, the waters are undersaturated with respect to smectite after injection, thus leading to dissolution. Conversely, waters from within the carbonate-only experiment (CarbCO₂) are not restricted to the quartz boundary and reaction paths move into the kaolinite stability field as a

result of a decrease in pH (increase in H⁺ activity) and increase in calcium activity; silicates are never saturated within the carbonate-only experiment. This change indicates that silica activity within the simulated carbonate reservoir is not controlled by the precipitation of quartz (Fig. 9). Theoretically, fluids from CarbCO₂ would continue reacting along the same path until the fluids ultimately reach the amorphous silica boundary.

The shale caprock is a larger potential source of metals compared to the limestone. However, more metals are removed from solution at the mixed shale-carbonate experiment (ShaleCO₂) compared to the carbonate-only experiment (CarbCO₂) due to precipitation of silicates and, possibly, adsorption onto clays. Waters within the simulated carbonate reservoir are saturated with respect to quartz but no other silicates. Therefore, the metal sink that is present at the simulated shale-carbonate reservoir interface does not exist in the carbonate-only experiment. Waters originating from deep within a carbonate reservoir may ultimately contain a greater trace metal load compared to waters in contact with shale at the top of a CO₂-charged

carbonate formation. This distinction becomes important when determining the potential impact of brine migration from different locations within a carbonate reservoir. If a package of water moves quickly from deep within the reservoir along a direct path (i.e. a poorly cemented wellbore or fault connecting two formations), the migration of metals and overall environmental impact has the potential to be larger than if fluids along the shale-carbonate reservoir contact migrate into a potable aquifer.

An Eh-pH diagram was constructed (Fig. 10) to understand how CO₂-water-rock interactions influence redox reactions and metal mobility. Iron activity is different in the two experiments, a_{Fe} is $10^{-4.5}$ to $10^{-5.3}$ in ShaleCO₂ and 10^{-6} in CarbCO₂; therefore, the Eh-pH diagram was constructed to bracket stability fields for these conditions. Note that the size of the aqueous field diminishes and the size of the mineral fields increase as the activity of iron increases. Eh was constrained by the aqueous geochemistry, experimental pressure and temperature, and mineral assemblage. Before the addition of CO₂, the reaction path for ShaleCO₂ and CarbCO₂ advances along the pyrite-hematite boundary at a_{Fe} of 10^{-5} and 10^{-4} , respectively, near the junction where pyrite-Fe-oxide-Fe²⁺(aq) stability fields meet. Data from the water-rock segment of ShaleCO₂ fall within the iron-oxide field (labeled here as hematite, but geochemical calculations using goethite provide the same result). In the parallel shale-carbonate reservoir experiment, in which CO₂ was not injected (ShaleBrine), secondary iron-oxides containing V, Co, and Ni are observed (Fig. 5A). Measured CO₂ and pH values approach steady state within 48 h after injection (Fig. 3). As a result, activities of aqueous species within individual samples in each experiment plot in groups (Fig. 10) suggesting that the majority of reaction progress occurs within the first 24–48 h; thus the initial segment of the reaction path in our experiments is not captured. If samples were collected within hours after injection, an understanding of initial CO₂-water-rock reactions and definition of the early reaction path might be possible.

The predicted pH value is slightly higher than the final in-situ pH value in both of the experiments (Fig. 3). This difference suggests that given more time the experiments would continue to approach equilibrium, secondary minerals would continue to form, and pH would continue to increase.

3.4.3. Multi-phase fluid (CO₂-brine)-rock interactions

Deep saline formations are rock-dominated, closed systems. These formations locally transition from rock-dominated to fluid-dominated systems in response to CO₂ injection, dramatically altering the nature of the geochemical reactions (Kaszuba and Janecky, 2009). Immediately after injection, CO₂ dissolution drives the geochemical reactions that were previously regulated by the host rock, as demonstrated in the activity diagrams (Figs. 8–10). Predicted concentrations reveal how different systems will recover after injection stops and the system can re-stabilize. With respect to the carbonate system (Fig. 8), fluids will eventually return to the same water-rock equilibrium state as before injection, and geochemical

reactions will again be governed by these carbonate minerals. Conversely, the silicate minerals and redox state of the experiments will not return to pre-injection conditions. This contrasting behavior is rooted in the reversibility of carbonate reactions versus the irreversibility of silicate reactions (Langmuir, 1997). It must be noted that pH and Eh of the experiment simulating the carbonate reservoir (CarbBrine) away from the caprock does not completely recover after acidification due to the time frames of these laboratory experiments, thus predicted pH and Eh values do not return to pre-injection conditions.

At 25 °C, bench pH for CarbBrine decreased slightly after CO₂-injection. Conversely, bench pH in ShaleBrine is observed to increase, a phenomenon also observed in arkose-shale experiments performed by Kaszuba et al. (2005). As a result of CO₂-brine interactions, carbonate and silicate minerals dissolved which produced an increase in alkalinity. At experimental conditions, however, increased alkalinity is overwhelmed by the acidity produced by dissolution of supercritical CO₂ and formation of carbonic acid. In the depressurized, cooled and degassed brine, supercritical CO₂ no longer dominates the fluid-rock system and the alkalinity neutralizes the acidity. The increase in bench pH is only observed in the shale-carbonate reservoir experiment due to the irreversible nature of the silicate reactions (Kaszuba and Janecky, 2009).

3.5. Implications for geologic systems

An understanding of trace metal evolution in a CO₂-charged carbonate reservoir and at the contact between the reservoir and a shale caprock provides knowledge of (1) secondary mineralization associated with long-term CO₂-water-rock interactions, and (2) information required for reliable assessment of risk associated with migration of water from a CO₂-charged formation into potable waters. Trace metals are especially important when evaluating the impact that fluids of contrasting redox behavior, such as formation waters bearing methane, carbon dioxide, or hydrogen sulfide, have on a carbonate formation and shale.

3.5.1. Potential impact to potable aquifers

Brine enriched in trace metals and saturated with CO₂ can impact an overlying potable aquifer in two ways. First, as the brine migrates upward and temperature and pressure decrease, CO₂ exsolves from the brine and subsequently dissolves into the aquifer. This process increases the acidity of water in the potable aquifer, leading to dissolution of carbonate minerals and release of additional trace metals into solution (i.e. Smyth et al., 2009; Little and Jackson, 2010; Karamalidis et al., 2013; Trautz et al., 2013). Exsolved CO₂ may also acidify waters along the flow path and potentially mobilize additional metals, such as those found in steel piping within the wellbore (Kharaka et al., 2009).

Second, trace metal solubility and mobility increase under acidic conditions. Our data suggests that Fe, Ni, and Pb concentrations in CO₂-saturated carbonate reservoir brine remain above EPA limits; if this brine migrates

into a potable aquifer, these three metals may warrant attention as potential contaminants of concern. However, at the contact between the carbonate reservoir and shale caprock, metals are more readily removed from solution by mineral precipitation and adsorption; only lead and iron exceed EPA limits. Additionally, lead concentrations could be further elevated by corrosion of well casing, as identified by [Kharaka et al. \(2009\)](#) in a field study of CO₂ injection into the Frio Sandstone. On the other hand, redox sensitive elements such as iron may not be a concern once mixed in oxygenated aquifers to potentially form new iron-oxides.

Migrating brine also possesses high TDS that makes potable water unsuitable for use without desalination and other filtration processes. Even with desalination, trace metals remain a concern for a number of reasons. These metals can be harmful at low concentrations, and thus small amounts have a big impact ([Environmental Protection Agency, 2012](#)). As the demand for water has skyrocketed with the increase in global population, societies are turning towards already scarce groundwater reserves to satisfy demands. Currently, the technology to desalinate water is available, but complex water chemistries containing important amounts of trace metals, salts, and organics are more energy intensive to treat. Metals can affect membrane efficiency, and thus removal of these constituents by secondary processes influences the overall cost of the water treatment ([Greenlee et al., 2009](#)).

3.5.2. Redox contrasts

Field studies in the Navajo Sandstone, the overlying potable aquifer in this region, ([Spangler et al., 1996](#); [Beitler et al., 2003, 2005](#); [Loope et al., 2010](#); [Wigley et al., 2012](#)) describe the geochemistry and mineralogy of contacts between white and red sandstones. These contacts are defined by accumulations of iron oxyhydroxide minerals and elevated concentrations of metals such as Co, Cu, Zn, Ni, Pb, Sn, Mo, U, and Cr. The contacts are interpreted as having formed at interfaces between two fluids that possess contrasting pH and redox potential, one a low pH, reducing, methane-bearing fluid and the other a higher pH, oxidizing, carbon dioxide-bearing fluid. Iron oxyhydroxide minerals such as hematite are stable in the oxidizing fluids but dissolve in the infiltrating reducing fluids; the red sandstone becomes white and metals dissolve into solution ([Loope et al., 2010](#); [Wigley et al., 2012](#)). Iron oxyhydroxide minerals reprecipitate at the interface with the oxidizing fluids, scavenging the metals from solution ([Wigley et al., 2012](#)). Our experiments demonstrate that pH and redox contrasts also drive metal mobility in carbonate reservoirs and shale caprocks. In these experiments, however, addition of CO₂ destabilizes pre-existing iron oxyhydroxides ([Figs. 7 and 10](#)). The pH decreases and the redox state of the system slightly increases, but the system evolves along the boundary between the pyrite and aqueous stability fields and away from the hematite stability field ([Figs. 7B and C](#)), liberating metals into solution ([Fig. 3](#)). Instead of reprecipitating along redox interfaces, the metals are scavenged from solution by precipitating pyrite. Copper and nickel, for example co-precipitate in secondary pyrite in ShaleCO₂ ([Fig. 6](#)). Geochemical calculations suggest that

siderite may also precipitate, providing an additional sink for metals.

3.5.3. CO₂–water–rock interactions in a carbonate formation and overlying shale

Our results are relevant for a variety of geologic environments in which a CO₂-charged carbonate reservoir is overlain by shale. Accumulations of supercritical CO₂ occur naturally on the Colorado Plateau and in the Rocky Mountains of the US, such as in the Madison Limestone of southwest Wyoming ([Pearce et al., 1996](#); [Allis et al., 2001](#); [Stevens et al., 2001](#); [Moore et al., 2005](#); [Gilfillan et al., 2009](#); [Kaszuba et al., 2011a](#)). Our experiments provide clues in relation to the evolution of natural waters and transformation of mineral assemblages that occurred following emplacement of CO₂ and formation of the natural reservoir. Anthropogenic activities, such as storing CO₂ in the subsurface and injecting CO₂ to enhance the recovery of oil and gas in petroleum systems, will also produce reservoirs of CO₂. Our work demonstrates the potential for secondary mineralization to help recapture mobilized metals as a consequence of CO₂–water–rock interactions in these environments.

The cooled, depressurized, and degassed brine that is produced after termination of our experiments yields clues to the possibility of additional secondary mineralization. If brine migrates into overlying formations, encountering lower temperatures and pressures and shifting redox potential, additional trace metals may be captured through the formation of these secondary minerals. After terminating experiments that simulate a shale–carbonate reservoir interface (ShaleBrine and ShaleCO₂), the brine became saturated with respect to Co-Fe and Zn oxides and Fe-Ni sulfides ([EA Table 4](#)). Terminating the experiments that simulate the deeper carbonate reservoir (CarbBrine and CarbCO₂) lead to brine becoming saturated with respect to Co-Fe and Zn-Cr oxides.

As observed in the shale in our experiments ([Fig. 5](#)), minerals dissolve, new minerals precipitate, and pore size apparently increases in response to CO₂ injection. Alteration of the mineralogy can make a shale caprock more susceptible to brittle deformation ([Lu et al., 2009](#); [Shukla et al., 2010](#)), thus potentially changing the overall integrity of the caprock. In contrast, studies of natural CO₂ reservoirs suggest that mudrocks are able to maintain seal integrity for geologically significant periods of time. In one example from the North Sea ([Lu et al., 2009](#)), CO₂ infiltrates only 0.3% of the seal in 70 Ma (12 meters in 70–80 Ma). Numerical GCS models also indicate that CO₂ only penetrates caprock 8 m in 3 Ka ([Gaus et al., 2005](#)). By analogy, a shale caprock may maintain its integrity and provide a considerable safety margin in a sequestration reservoir, even though pores appear to increase in size from geochemical reactions at the shale–carbonate reservoir contact ([Shipton et al., 2004](#); [May, 2005](#)). By analogy to the observations of [Lu et al. \(2009\)](#), the overall permeability of the caprock through the entire thickness may not change.

The water–rock experiments without supercritical CO₂ (ShaleBrine and CarbBrine) provide insight into trace metal mobilization and secondary mineralization as a

consequence of injection of hot water and steam to enhance the recovery of oil and gas in petroleum systems. Not surprisingly, water–rock interactions in these environments dissolve reservoir minerals and mobilize trace metals. In our experiments, most of these metals co-precipitate with secondary minerals but Ba, Fe, Ni, and Pb concentrations remain elevated.

3.5.4. Unconventional oil and gas reservoirs

The development of unconventional shale gas and shale oil resources through hydraulic fracturing shares several attributes with geologic storage of CO₂ in the subsurface (Nicot and Duncan, 2012). These commonalities include introducing acidic fluids into geologic units, potentially mobilizing metals and other constituents, and a subsequent potential for impacting potable groundwater through leakage of formation waters. Hydraulic fracturing fluid remains in the formation for as little as 1–3 days (Andrews et al., 2009; King, 2012), which is the time frame for the majority of the reactions observed in our experiments. Acidic hydraulic fracturing fluids react with calcareous shales (marls) or pelitic shales in unconventional reservoirs, reactions broadly comparable to the reaction of acidic, carbonated formation waters with carbonate rock and shale in our experiments. While the aqueous fluid chemistry of the two systems differs in detail, acid reactions dominate both, at least initially. In the absence of studies that evaluate the evolution of trace metals in a hydraulically fractured formation, our results provide clues regarding fluid–rock interactions induced by hydraulic fracturing. In response to acidity, our shale-bearing experiments suggest that Fe, Ni, Pb, and Cu may be mobilized within days of injecting acidic fluids. Over time, iron is reincorporated into the rocks, whereas Ni, Pb, and Cu concentrations in formation waters continue to increase. These experimental trends are broadly similar to trends described in a study of produced waters from the Marcellus Shale (Rowen et al., 2015). Our experiments also suggest that swelling clays (smectites) may form in response to injection of acidic fluids, a development that could adversely impact the engineered micro-fracture network.

5. CONCLUSIONS AND RECOMMENDATIONS FOR FUTURE WORK

This experimental investigation evaluates the effect of CO₂–brine–rock interactions on the evolution of trace metals and on secondary mineralization in a simulated carbonate reservoir charged with CO₂ and overlain by shale. Mobilization of trace metals and precipitation of secondary minerals constrain fluid–rock interactions in a wide range of geochemical environments including CO₂ storage reservoirs for GCS, petroleum systems in which CO₂ is injected to enhance the recovery of oil and gas, enhanced geothermal systems using CO₂ as the working fluid, the development of unconventional shale gas and shale oil reservoirs, naturally-occurring CO₂ reservoirs, CO₂-bearing petroleum systems, and CO₂-charged thermal springs. An understanding of the mobilization of trace metals that are potentially deleterious to human health and the environment is critical

for analyzing potential risks associated with anthropogenic CO₂ systems.

Hydrothermal experiments investigated two locations within a theoretical shale-carbonate reservoir sequence: at the shale–carbonate interface and in the carbonate reservoir away from the caprock. Addition of supercritical CO₂ decreased brine pH by 1 to 2 units and increased the concentrations of metals in solution. In the carbonate-only experiment, carbonate minerals react with the acidic brine releasing Ba, Cd, Co, Cu, Cr, Fe, Ni, Pb, V, and Zn into solution. Concentrations of these metals generally decreased 120–330 h after injection and approached steady state values due to precipitation of secondary sulfides and clays.

In the mixed shale-carbonate experiment, carbonate and silicate minerals react and release Cd, Co, Cu, Cr, Fe, Ni, Pb, V, and Zn into solution at concentrations higher than those observed in the carbonate-only experiment. However, 72 h after injection, metals concentrations decreased to values near or lower than concentrations observed in the carbonate-only experiment. Even though the shale caprock provides a greater source of metals, it has an active role in trace metal evolution by providing secondary smectites and other silicates as additional metal sinks. Secondary silicates are not found within a carbonate reservoir away from the caprock, eliminating this potential sink. The experiments are validated by analogous secondary mineralization that is consistent with mineralization in faults and fractures at the contact of the limestone-shale sequence on which the experiments are based.

At the conclusion of both experiments injected with supercritical CO₂, iron, an element of secondary concern, lead, and chromium remained above EPA limits (approximately 1500–1800 h). Nickel, an element regulated by WHO, and vanadium concentrations remained elevated after injection. Decreasing trends of iron and lead concentrations in the mixed shale-carbonate experiment, and lead and vanadium in the carbonate-only experiment, suggest these trace metals become less of an environmental concern as CO₂-water–rock reactions evolve with time. Additionally, zinc exceeds the limits at the simulated shale-carbonate contact and Ba, Cu, and Cd exceed the limits in the carbonate-only experiment. Several trace metals that were initially mobilized in response to CO₂-water–rock reactions are recaptured by precipitation of secondary minerals and adsorption processes. This potential self-healing mechanism could mitigate, but not eliminate, the potential impact of trace metals in carbon sequestration scenarios and other CO₂-charged systems. The importance of secondary minerals on trace metal evolution underscores the importance developing a complete understanding of the mineralogy and petrology of an anthropogenic system prior to introducing CO₂.

As an important direction of future work, we recommend kinetic and reactive transport modeling to investigate time scales and rates at which metals are mobilized and removed from solution and to develop an understanding of metal evolution within a natural system. Our study focused on mineralogy and inorganic geochemistry; experimental investigation of the organic geochemistry could

provide valuable information on the role of organic matter in the evolution of trace metals. Adsorption experiments and use of various spectroscopies could evaluate the relative importance of metal co-precipitation in secondary minerals and sorption on mineral surfaces.

ACKNOWLEDGEMENTS

This project was supported by an EPA Star Grant R834387 to Kaszuba (UW) and to J. McCray, R. J. Maxwell, and A. Stichler at the Colorado School of Mines, and by a McMurry Fellowship in Energy Research in Geology and Geophysics scholarship to Marcon. John Kaszuba's work was also supported by the UW School of Energy Resources. We acknowledge The Laboratory for Environmental and Geological Studies (LEGS) at the University of Colorado, particularly Fredrick G. Luiszer, for aqueous analyses and Jason Heath for supplying the Gothic Shale samples. We thank Susan Swapp and Norbert Swoboda-Colberg for assistance with XRD and SEM analyses, Kellie Antrobus and Ryan Herz-Thyhsen for performing BET measurements at the University of Wyoming, Michael Marcon for guidance with statistical analyses, and Caroline Lo Ré for all the laboratory assistance. We thank Drs. Geoffrey Thyne and Dennis Newell for reviews of an earlier version of this paper. We also thank the Executive Editor, the Associate Editor, and four anonymous reviewers for their thoughtful reviews.

APPENDIX A. SUPPLEMENTARY DATA

Supplementary data associated with this article can be found, in the online version, at <http://dx.doi.org/10.1016/j.gca.2015.06.037>.

REFERENCES

- Alemu B. L., Aagaard P., Munz I. A. and Skurtveit E. (2011) Caprock interaction with CO₂: a laboratory study of reactivity of shale with supercritical CO₂ and brine. *Appl. Geochem.* **26**, 1975–1989.
- Allis, T., Chidsey, T., Gwynn, W., Morgan, C., White, S., Adams, M. and Moore, J. (2001) Natural CO₂ Reservoirs on the Colorado Plateau and Southern Rocky Mountains: Candidates for CO₂ Sequestration. First National Conference on Carbon Sequestration. National Energy Technology Laboratory, Washington D.C.
- Anderson G. M. and Crerar D. A. (1993) *Thermodynamics in Geochemistry- The Equilibrium Model*. Oxford University Press.
- Andrews, A., Folger, P., Humphries, M., Copeland, C., Tiemann, M., Meltz, R. and Brougher, C. (2009) Unconventional Gas Shales: Development, Technology, and Policy Issues, Congressional Research Service Report for Congress. Congress, <<http://www.crs.gov>>.
- Avery C. (1986) *Bedrock Aquifers of Eastern San Juan County, Utah*. Utah Water Science Center, Salt Lake City, UT, p. 124.
- Bandstra J. Z. and Brantley S. L. (2008) Data fitting techniques with applications to mineral dissolution kinetics. In *Kinetics of Water–Rock Interaction* (eds. S. L. Brantley, J. D. Kubicki and A. F. White). Springer Science Business Media, New York, pp. 211–257.
- Bearup L. A., Navarre-Stichler A. K., Maxwell R. M. and McCray J. E. (2012) Kinetic metal release from competing processes in aquifers. *Environ. Sci. Technol.* **46**, 6539–6547.
- Beitler B., Chan M. and Parry W. (2003) Bleaching of Jurassic Navajo Sandstone on Colorado Plateau Laramide highs: evidence of exhumed hydrocarbon supergiants?. *Geology* **31** 1041–1044.
- Beitler B., Parry W. T. and Chan M. A. (2005) Fingerprints of fluid flow: chemical diagenetic history of the Jurassic Navajo Sandstone, Southern Utah, USA. *J. Sediment. Res.* **75**, 547–561.
- Benson S. M. and Cole D. R. (2008) CO₂ sequestration in deep sedimentary formations. *Elements* **4**, 325–331.
- Bethke, C. and Yeakel, S. (2012) The Geochemist Workbench Release 9.0. Champaign, Illinois.
- Birkholzer J. T. and Zhou Q. (2009) Basin-scale hydrogeologic impacts of CO₂ storage: capacity and regulatory implications. *Int. J. Greenh. Gas Con.* **3**, 745–756.
- Birkholzer J. T., Zhou Q. and Tsang C.-F. (2009) Large-scale impact of CO₂ storage in deep saline aquifers: a sensitivity study on pressure response in stratified systems. *Int. J. Greenh. Gas Con.* **3**, 181–194.
- Callahan J. and Marcon M. (2013) *Qual Stat (6)*. Houston, TX.
- Chopping C. and Kaszuba J. P. (2012) Supercritical carbon dioxide-brine-rock reactions in the Madison Limestone of Southwest Wyoming: an experimental investigation of a sulfur-rich natural carbon dioxide reservoir. *Chem. Geol.* **322**, 223–236.
- Collins A. G. (1975) *Geochemistry of Oilfield Waters*. Elsevier Scientific Publishing Company, Amsterdam.
- Creodoz A., Bildstein O., Jullien M., Raynal J., Pétronin J.-C., Lillo M., Pozo C. and Geniaut G. (2009) Experimental and modeling study of geochemical reactivity between clayey caprocks and CO₂ in geological storage conditions. *Energ. Procedia* **1**, 3445–3452.
- DePaolo D. J., Cole D. R., Navrotsky A. and Bourg I. C. (2013) Geochemistry of Geologic CO₂ sequestration. In *Reviews in Mineralogy & Geochemistry* (ed. J. J. Rosso). The Mineralogical Society of America, Chantilly, Virginia, p. 539.
- Drever J. (1997) *The Geochemistry of Natural Waters: Surface and Groundwater Environments*, third ed. Prentice-Hall, Upper Saddle River.
- Duan Z. H., Sun R., Zhu C. and Chou I. M. (2006) An improved model for the calculation of CO₂ solubility in aqueous solutions containing Na⁺, K⁺, Ca²⁺, Mg²⁺, Cl⁻, and SO₄²⁻. *Mar. Chem.* **98**, 131–139.
- Environmental Protection Agency (2012) Drinking Water Contaminants. 2013, <<http://water.epa.gov/drink/contaminants/>>.
- European Parliament and Council (2000) Directive 2000/60/EC of The European Parliament and of the Council, 2000L0060. European Parliament and the Council of the European Union OJ L 327.
- Gaus I., Azaroual M. and Czernichowski-Lauriol I. (2005) Reactive transport modelling of the impact of CO₂ injection on the clayey cap rock at Sleipner (North Sea). *Chem. Geol.* **217**, 319–337.
- Gilfillan S. M. V., Lollar B. S., Holland G., Blagburn D., Stevens S., Schoell M., Cassidy M., Ding Z., Zhou Z., Lacrampe-Couloume G. and Ballentine C. J. (2009) Solubility trapping in formation water as dominant CO₂ sink in natural gas fields. *Nature* **458**, 614–618.
- Goldammer, R. K., Oswald, E. J. and Dunn, P. A. (1994) High-frequency, glacio-eustatic cyclicity in the Middle Pennsylvanian of the Paradox Basin: An evaluation of Milankovitch forcing. Special Publication International Association of Sedimentologists, 19, pp. 243–283.

- Goode, H.D. (1958) The geology and distribution of aquifers in the Southeastern Part of San Juan County, Utah. U.S. Geological Survey Open File Report 58-38, 9p.
- Greenlee L. F., Lawler D. F., Freeman B. D., Marrot B. and Moulin P. (2009) Reverse osmosis desalination: water sources, technology, and today's challenges. *Water Res.* **43**, 2317–2348.
- Griffith C. A., Dzombak D. A. and Lowry G. V. (2011) Physical and chemical characteristics of potential seal strata in regions considered for demonstrating geological saline CO₂ sequestration. *Environ. Earth Sci.* **64**, 925–948.
- Gunter W. D., Wivchar B. and Perkins E. H. (1997) Aquifer disposal of CO₂-rich greenhouse gases: extension of the time scale of experiment for CO₂-sequestering reactions by geochemical modelling. *Miner. Petrol.* **59**, 121–140.
- Han W. S., Lu M., McPherson B. J., Keating E. H., Moore J., Park E., Watson Z. T. and Jung N. H. (2013) Characteristics of CO₂-driven cold-water geyser, Crystal Geyser in Utah: experimental observation and mechanism analyses. *Geofluids* **13**, 283–297.
- Heath J. E., Dewers T. A., McPherson B. J. O. L., Petrusak R., Chidsey, Jr., T. C., Rinehart A. J. and Mozley P. S. (2011) Pore networks in continental and marine mudstones: characteristics and controls on sealing behavior. *Geosphere* **7**, 429–454.
- Hitzman, M., Kirkham, R., Broughton, D., Thorson, J. and Selley, D. (2005) The sediment-hosted stratiform copper ore system, In *Economic Geology* (eds. J. W. Hedenquist, J. F. H. Thompson, R. J. Goldfarb, J. P. Richards). pp. 609–642.
- Humez P., Audigane P., Lions J., Négrel P. and Lagneau V. (2011) Tracking and CO₂ leakage from deep saline to fresh groundwaters: development of sensitive monitoring techniques. *Energ. Procedia* **4**, 3443–3449.
- Humez P., Lagneau V., Lions J. and Négrel P. (2013) Assessing the potential consequences of CO₂ leakage to freshwater resources: a batch-reaction experiment towards an isotopic tracing tool. *Appl. Geochem.* **30**, 178–190.
- Humez P., Négrel P., Lagneau V., Lions J., Kloppmann W., Gal F., Millot R., Guerrot C., Flehoc C., Widory D. and Girard J.-F. (2014) CO₂-water-mineral reactions during CO₂ leakage: geochemical and isotopic monitoring of a CO₂ injection field test. *Chem. Geol.* **368**, 11–30.
- IPCC (2005) IPCC Special Report on Carbon Dioxide Capture and Storage, In (eds. B. Metz, O. Davidson, H. d. Coninck, M. Loos, L. Meyer). Cambridge, United Kingdom and New York, NY.
- Karamalidis A. K., Torres S. G., Hakala J. A., Shao H. B., Cantrell K. J. and Carroll S. (2013) Trace metal source terms in carbon sequestration environments. *Environ. Sci. Technol.* **47**, 322–329.
- Kaszuba J. P. and Janecky D. R. (2009) Geochemical impacts of sequestering carbon dioxide in brine formations. In *Carbon Sequestration and its Role in the Global Carbon Cycle* (eds. E. Sundquist and B. McPherson). American Geophysical Union, Washington, DC, pp. 239–247.
- Kaszuba J. P., Janecky D. R. and Snow M. G. (2003) Carbon dioxide reaction processes in a model brine aquifer at 200 °C and 200 bars: implications for geologic sequestration of carbon. *Appl. Geochem.* **18**, 1065–1080.
- Kaszuba J. P., Janecky D. R. and Snow M. G. (2005) Experimental evaluation of mixed fluid reactions between supercritical carbon dioxide and NaCl brine: relevance to the integrity of a geologic carbon repository. *Chem. Geol.* **217**, 277–293.
- Kaszuba J. P., Navarre-Sitchler A., Thyne G., Chopping C. and Meuzelaar T. (2011a) Supercritical carbon dioxide and sulfur in the Madison Limestone: a natural analog in southwest Wyoming for geologic carbon-sulfur co-sequestration. *Earth Planet. Sci. Lett.* **309**, 131–140.
- Kaszuba J. P., Viswanathan H. S. and Carey J. W. (2011b) Relative stability and significance of dawsonite and aluminum minerals in geologic carbon sequestration. *Geophys. Res. Lett.*, 38.
- Keating E. H., Fessenden J., Kanjorski N., Koning D. J. and Pawar R. (2010) The impact of CO₂ on shallow groundwater chemistry: observations at a natural analog site and implications for carbon sequestration. *Environ. Earth Sci.* **60**, 521–536.
- Keating E. H., Hakala J. A., Viswanathan H., Carey J. W., Pawar R., Guthrie G. D. and Fessenden-Rahn J. (2013a) CO₂ leakage impacts on shallow groundwater: field-scale reactive-transport simulations informed by observations at a natural analog site. *Appl. Geochem.* **30**, 136–147.
- Keating E. H., Newell D. L., Viswanathan H., Carey J. W., Zylowski G. and Pawar R. (2013c) CO₂/brine transport into shallow aquifers along fault zones. *Environ. Sci. Technol.* **47**, 290–297.
- Kharaka Y. K., Thordsen J. J., Hovorka S. D., Seay Nance H., Cole D. R., Phelps T. J. and Knauss K. G. (2009) Potential environmental issues of CO₂ storage in deep saline aquifers: geochemical results from the Frio-I Brine Pilot test, Texas, USA. *Appl. Geochem.* **24**, 1106–1112.
- Kharaka Y. K., Thordsen J. J., Kakouros E., Ambats G., Herkelrath W. N., Beers S. R., Birkholzer J. T., Apps J. A., Spycher N. F., Zheng L., Trautz R. C., Rauch H. W. and Gullickson K. S. (2010) Changes in the chemistry of shallow groundwater related to the 2008 injection of CO₂ at the ZERT field site, Bozeman, Montana. *Environ. Earth Sci.* **60**, 273–284.
- King, G. E. (2012) Hydraulic Fracturing 101: What Every Representative, Environmentalist, Regulator, Reporter, Investor, University Researcher, Neighbor and Engineer Should Know About Estimating Frac Risk and Improving Frac Performance in Unconventional Gas and Oil Wells. In *Society of Petroleum Engineers* (ed.), SPE Hydraulic Fracturing Technology Conference. SPE, Woodlands, TX.
- Kirsch K., Navarre-Sitchler A. K., Wunsch A. and McCray J. E. (2014) Metal release from sandstones under experimentally and numerically simulated CO₂ leakage conditions. *Environ. Sci. Technol.* **48**, 1436–1442.
- Krauskopf, K. B. and Bird, D. K. (1994) Introduction To Geochemistry, third ed. McGraw-Hill Science/Engineering/Math.
- Langmuir D. (1997) *Aqueous Environmental Geochemistry*. Prentice Hall, Upper Saddle River.
- Leach, D. L., Sangster, D. F., Kelley, K. D., Large, R. R., Garven, G., Allen, C. R., Gutzmer, J. and Walters, S. (2005) Sediment-hosted lead-zinc deposit: A global perspective. In *Economic Geology* (eds. J. W. Hedenquist, J. F. H. Thompson, R. J. Goldfarb, J. P. Richards). pp. 609–642.
- Lions J., Devau N., de Lary L., Dupraz S., Parmentier M., Gombert P. and Dictor M.-C. (2014) Potential impacts of leakage from CO₂ geological storage on geochemical processes controlling fresh groundwater quality: a review. *Int. J. Greenh. Gas Con.* **22**, 165–175.
- Little M. G. and Jackson R. B. (2010) Potential impacts of leakage from deep CO₂ geosequestration on overlying freshwater aquifers. *Environ. Sci. Technol.* **44**, 9225–9232.
- Liu F., Lu P., Griffith C., Hedges S. W., Soong Y., Hellevang H. and Zhu C. (2012) CO₂-brine-caprock interaction: reactivity experiments on Eau Claire shale and a review of relevant literature. *Int. J. Greenh. Gas Con.* **7**, 153–167.
- Loope D. B., Kettler R. M. and Weber K. A. (2010) Follow the water: connecting a CO₂ reservoir and bleached sandstone to iron-rich concretions in the Navajo Sandstone of south-central Utah, USA. *Geology* **38**, 999–1002.

- Lu J., Wilkinson M., Haszeldine R. S. and Fallick A. E. (2009) Long-term performance of a mudrock seal in natural CO₂ storage. *Geology* **37**, 35–38.
- Lu J., Wilkinson M., Haszeldine R. S. and Boyce A. J. (2010a) Carbonate cements in Miller field of the UK North Sea: a natural analog for mineral trapping in CO₂ geological storage. *Environ. Earth Sci.* **62**, 507–517.
- Lu P., Fu Q., Seyfried W. E., Hereford A. and Zhu C. (2010b) Navajo Sandstone–brine–CO₂ interaction: implications for geological carbon sequestration. *Environ. Earth Sci.* **62**, 101–118.
- Manrique E., Gurfinkel M. and Muci V. (2004) *Enhanced oil recovery field experiences in carbonate reservoirs in the United States, 25th Annual Workshop & Symposium Collaborative Project on Enhanced Oil Recovery International Energy Agency*. International Energy Agency, Stavanger, Norway.
- Marcon V. (2013) *Carbon dioxide–Water–Rock Interaction in a Carbonate Reservoir Capped by Clay: An Experimental Investigation on the Evolution of Trace Metals*. M.Sc. University of Wyoming.
- May F. (2005) Alteration of wall rocks by CO₂-rich water ascending in fault zones. *Oil Gas Sci. Technol.* **60**, 19–32.
- McClure, K., Morgan, C., Thomas Chidsey, J., Survey, U. G. and Eby, D. (2003) Heterogeneous shallow-shelf carbonate buildups in the Paradox Basin, Utah and Colorado: Targets for increased oil production and reserves using horizontal drilling techniques. In (ed. G.D. Walker), Deliverable 1.1.1 Regional Paradox Formation Structure and Isochore Maps, Blanding Sub-Basin, Utah. Utah Geological Survey, Salt Lake City.
- Moore J., Adams M., Allis R., Lutz S. and Rauzi S. (2005) Mineralogical and geochemical consequences of the long-term presence of CO₂ in natural reservoirs: an example from the Springerville–St. Johns Field, Arizona, and New Mexico, USA. *Chem. Geol.* **217**, 365–385.
- New Mexico Tech (2012a) Phase II Results. 2014, <http://www.southwestcarbonpartnership.org/index.php?option=com_content&view=article&id=100&Itemid=506>.
- New Mexico Tech (2012b) Southwest Partnership: CO₂ Sequestration. 2013, <<http://www.southwestcarbonpartnership.org/>>.
- Newell D. L., Kaszuba J. P., Viswanathan H. S., Pawar R. J. and Carpenter T. (2008) Significance of carbonate buffers in natural waters reacting with supercritical CO₂: implications for monitoring, measuring and verification (MMV) of geologic carbon sequestration. *Geophys. Res. Lett.*, **35**.
- Nicot J.-P. and Duncan I. J. (2008) Science-based permitting of geological sequestration of CO₂ in brine reservoirs in the US. *Environ. Sci. Policy* **11**, 14–24.
- Nicot J.-P. and Duncan I. J. (2012) Common attributes of hydraulically fractured oil and gas production and CO₂ geological sequestration. *Greenh. Gas. Sci. Technol.* **2**, 352–368.
- Pearce J. M., Holloway S., Wacker H., Nelis M. K., Rochelle C. and Bateman K. (1996) Natural occurrences as analogues for the geological disposal of carbon dioxide. *Energ. Convers.* **37**, 1123–1128.
- Pruess K. (2006) Enhanced geothermal systems (EGS) using CO₂ as working fluid: a novel approach for generating renewable energy with simultaneous sequestration of carbon. *Geothermics* **35**, 351–367.
- Qafoku O., Kovarik L., Kukkadapu R. K., Ilton E. S., Arey B. W., Tucek J. and Felmy A. R. (2012) Fayalite dissolution and siderite formation in water-saturated supercritical CO₂. *Chem. Geol.* **332**, 124–135.
- Rempel K. U., Liebscher A., Heinrich W. and Schettler G. (2011) An experimental investigation of trace element dissolution in carbon dioxide: applications to the geological storage of CO₂. *Chem. Geol.* **289**, 224–234.
- Rillard J., Gombert P., Toulhoat P. and Zuddas P. (2014) Geochemical assessment of CO₂ perturbation in a shallow aquifer evaluated by a push–pull field experiment. *Int. J. Greenh. Gas Con.* **21**, 23–32.
- Rowen E. L., Engle M. A., Kraemer T. F., Schroeder K. T., Hammack R. W. and Doughten M. W. (2015) Geochemical and isotopic evolution of water produced from Middle Devonian Marcellus shale gas wells, Appalachian basin, Pennsylvania. *AAPG Bull.* **99**, 181–206.
- Rutledge, J. (2010) Geologic Demonstration at the Aneth Oil Field, Paradox Basin, Utah, Southwest Regional Partnership on Carbon Sequestration Phase II. New Mexico Institute of Mining and Technology and Los Alamos National Laboratory, Socorro.
- Sarg J. (1999) The sequence stratigraphy, sedimentology, and economic importance of evaporite±carbonate transitions- a review. *Sediment. Geol.* **140**, 9–42.
- Schaefer F., Walter L., Class H. and Mueller C. (2012) The regional pressure impact of CO₂ storage: a showcase study from the North German Basin. *Environ. Earth Sci.* **65**, 2037–2049.
- Schoonen M. A. A., Sklute E. C., Dyar M. D. and Strongin D. R. (2012) Reactivity of sandstones under conditions relevant to geosequestration: 1. Hematite-bearing sandstone exposed to supercritical carbon dioxide commingled with aqueous sulfite or sulfide solutions. *Chem. Geol.* **296**, 96–102.
- Seyfried W., Janecky D. and Berndt M. (1987) Rocking autoclaves for hydrothermal experiments II: the flexible reaction-cell system. In *Hydrothermal Experimental Techniques* (eds. G. Ulmer and H. Barnes). John Wiley & Sons, New York, pp. 216–239.
- Shipton, Z.K., Evans, J.P., Kirchner, D., Kolesar, P.T., Williams, A.P. and Heath, J. (2004) Analysis of CO₂ leakage through “low-permeability” faults from natural reservoirs in the Colorado Plateau, southern Utah, in: Baines, S.J., Worden, R.H. (Eds.), *Geologic Storage of Carbon Dioxide*. London Special Publication, Geological Society, pp. 43–58.
- Shukla R., Ranjith P., Haque A. and Choi X. (2010) A review of studies on CO₂ sequestration and caprock integrity. *Fuel* **89**, 2651–2664.
- Smyth R. C., Hovorka S. D., Lu J., Romanak K. D., Partin J. W., Wong C. and Yang C. (2009) Assessing risk to fresh water resources from long term CO₂ injection–laboratory and field studies. *Energ. Procedia* **1**, 1957–1964.
- Spangler L. E., Naftz D. L. and Peterman Z. E. (1996) Hydrology, Chemical Quality, and Characterization of Salinity in the Navajo Aquifer in and near the Greater Aneth Oil Field, San Juan County, Utah. In *Water-Resources Investigations Report* (ed. B. Babbitt). USGS, Salt Lake City, Utah, pp. 227–239.
- Stevens, S. H., Pearce, J. M. and Rigg, A. A. J. (2001) Natural analogs for geologic storage of CO₂: an integrated global research program, First National Conference on Carbon Sequestration. U.S. Department of Energy, Washington, D.C.
- Trautz R. C., Pugh J. D., Varadharajan C., Zheng L., Bianchi M., Nico P. S., Spycher N. F., Newell D. L., Esposito R. A., Wu Y., Dafflon B., Hubbard S. S. and Birkholzer J. T. (2013) Effect of dissolved CO₂ on a shallow groundwater system: a controlled release field experiment. *Environ. Sci. Technol.* **47**, 298–305.
- Tucker M. E. and Wright V. P. (1990) *Carbonate Sedimentology*. Blackwell Science Ltd, Malden, MA.
- Tuttle M., Klett T., Richardson M. and Breit G. (1996) Geochemistry of two interbeds in Pennsylvanian Paradox Formation, Utah and Colorado: a record of deposition and diagenesis of repetitive cycles in a marine basin. In *Evolution of*

- (ed. A. C. Huffman). U.S. Geological Survey, Denver, pp. N4–N6.
- Walter L., Binning P. J., Oladyskhin S., Flemisch B. and Class H. (2012) Brine migration resulting from CO₂ injection into saline aquifers – an approach to risk estimation including various levels of uncertainty. *Int. J. Greenh. Gas Con.* **9**, 495–506.
- Wang S. and Jaffe P. R. (2004) Dissolution of a mineral phase in potable aquifers due to CO₂ releases from deep formations; effect of dissolution kinetics. *Energy Convers. Manage.* **45**, 2833–2848.
- Wigley M., Kampman N., Dubacq B. and Bickle M. (2012) Fluid-mineral reactions and trace metal mobilization in an exhumed natural CO₂ reservoir, Green River, Utah. *Geology* **40**, 555–558.
- Wilkin R. T. and Digiulio D. C. (2010) Geochemical impacts to groundwater from geologic carbon sequestration: controls on pH and inorganic carbon concentrations from reaction path and kinetic modeling. *Environ. Sci. Technol.* **44**, 4821–4827.
- World Health Organization (2011) *Guidelines for Drinking-water Quality*. WHO Press, World Health Organization, Geneva, Switzerland.
- Wunsch A., Navarre-Sitchler A. K. and McCray J. E. (2013a) Geochemical implications of brine leakage into freshwater aquifers. *Ground Water* **51**, 855–865.
- Wunsch A., Navarre-Sitchler A. K., Moore J. and McCray J. E. (2013c) Metal release from limestones at high partial-pressures of CO₂. *Chem. Geol.* **363**, 40–55.
- Wunsch A., Navarre-Sitchler A. K., Moore J., Ricko A. and McCray J. E. (2013f) Metal release from dolomites at high partial-pressures of CO₂. *Appl. Geochem.* **38**, 33–47.
- Xu T. F., Apps J. A. and Pruess K. (2004) Numerical simulation of CO₂ disposal by mineral trapping in deep aquifers. *Appl. Geochem.* **19**, 917–936.
- Xu T. F., Apps J. A. and Pruess K. (2005) Mineral sequestration of carbon dioxide in a sandstone-shale system. *Chem. Geol.* **217**, 295–318.
- Xu T., Apps J. A., Pruess K. and Yamamoto H. (2007) Numerical modeling of injection and mineral trapping of CO₂ with H₂S and SO₂ in a sandstone formation. *Chem. Geol.* **242**, 319–346.
- Zheng L., Apps J. A., Zhang Y., Xu T. and Birkholzer J. T. (2009) On mobilization of lead and arsenic in groundwater in response to CO₂ leakage from deep geological storage. *Chem. Geol.* **268**, 281–297.

Associate editor: Brian W. Stewart